# A Framework to Avoid Maloperation of Transformer Differential Protection Under Geomagnetic Disturbances

by

Mehdi Zandian

A thesis submitted in partial fulfillment for the
Master of Science degree

in the
Faculty of Graduate Studies
Electrical Engineering Department

May 2023

# Declaration of Authorship

I, Mehdi Zandian, declare that this thesis titled, "A Framework to Avoid Maloperation of Transformer Differential Protection Under Geomagnetic Disturbances" and the work presented in it are my own. I confirm that:

- This work was done wholly or mainly while in candidature for a research degree at this University.
- Where any part of this thesis has previously been submitted for a degree or any other qualification at this University or any other institution, this has been clearly stated.
- Where I have consulted the published work of others, this is always clearly attributed.
- Where I have quoted from the work of others, the source is always given. With the exception of such quotations, this thesis is entirely my own work.
- I have acknowledged all main sources of help.
- Where the thesis is based on work done by myself jointly with others, I have made clear exactly what was done by others and what I have contributed myself.

Signed: Mehdi Zandian

Date: April 11, 2023

*"To go beyond your capacity: sure, why not, and most likely doable. However, at the expensive cost of losing parts of yourself. "*

(The Great Sina)

# *Abstract*

Geomagnetically Induced Currents (GICs), which are generated due to Geomagnetic Disturbances (GMDs), can saturate the cores of power transformers and their associated Current Transformers (CTs). To avoid maloperation of Transformer Differential relays in the presence of GICs, this family of relays is often equipped with Harmonic Blocking (HB) or Harmonic Restrain (HR) functions. These two functions, however, negatively impact the sensitivity and dependability of differential relays during GICs. Thus, if an internal fault occurs in the presence of GICs, it might remain uninterrupted. On this basis, this study proposes an auxiliary framework for single-phase transformers or three-phase transformer banks to address the above-mentioned issues for differential relays and their CTs without sacrificing the sensitivity and/or speed of differential protection. This framework benefits from the Linear Parameter Varying (LPV) state-space equations of CTs and power transformers, and convert them to their polytopic form. Then, it employs LPV observers to estimate the states of the transformer and its CTs. To counter CT saturation, the framework precisely calculates the primary currents of CTs based on their secondary currents, allowing the differential scheme to use the estimated primary currents rather than distorted secondary currents. Furthermore, the proposed framework detects internal faults by comparing the estimated primary current of the transformer with the measured one. The difference between the estimated and measured currents is almost zero when no internal fault is present during GMDs; however, the discrepancy between the two grows as soon as an internal fault occurs. The effectiveness of the proposed framework is validated through simulations in Electromagnetic Transient Program (EMTP).

# *Acknowledgements*

I would like to express my sincere appreciation and absolute gratitude to my supervisor, Dr. Amir Ameli. This research would not have been possible without his insights, guidance, and dedication in teaching and supporting me during my research. I would also like to thank Dr. Mohsen Ghafouri from the Concordia Institute for Information Systems Engineering, Concordia University, Montreal, for the expertise and support he provided me with this research.

My respect and thankfulness goes to my committee members at Lakehead University, Dr. Carlos Christoffersen, Dr. Apparao Dekka, and Graduate Coordinator Dr. Yushi Zhou at Electrical Engineering Department, who have examined my research.

I am thankful to Lakehead University for its invaluable support through the scholarships I have been awarded. The scholarships helped alleviate the financial burden and enabled me to pursue my academic journey with greater ease.

My extreme gratitude goes to my family who have supported me patiently and encouraged me towards my education.

# Contents

# List of Figures

# List of Tables

# Abbreviations

| | |
|---|---|
| **CIR** | **C**o-Rotating **I**nteraction **R**egion |
| **CME** | **C**oronal **M**ass **E**jection |
| **CT** | **C**urrent **T**ransformer |
| **DC** | **D**irect **C**urrent |
| **GEF** | **G**eo-**E**lectric **F**ield |
| **GIC** | **G**eomagnetically **I**nduced **C**urrent |
| **GMD** | **G**eomagnetic **D**isturbance |
| **GPS** | **G**lobal **P**ositioning **S**ystem |
| **HB** | **H**armonic **B**locking |
| **HR** | **H**armonic **R**estraining |
| **LTI** | **L**inear **T**ime **I**nvariant |
| **LPV** | **L**inear **P**arameter **V**arying |
| **ML** | **M**achine **L**earning |
| **QS** | **Q**uadratic **S**tability |
| **SSC** | **S**udden **S**torm **C**ommencement |
| **SS** | **S**tate **S**pace |
| **TT** | **T**urn to **T**urn |
| **TG** | **T**urn to **G**round |
| **87T** | Transformer Differential Protection Relay |

# Symbols

| | |
|---|---|
| $A$ | Magnetic Potential Vector |
| $B$ | Magnetic Flux Density |
| $Dst$ | Disturbance Storm-Time Index |
| $E$ | Electric Field |
| $f_{87T}(.)$ | 87T Characteristic function |
| $G$ | Observer Z state input gain |
| $H$ | Observer $\hat{x}$ state feedback gain |
| $I_{diff}$ | Differential Current in 87T |
| $I_{res}$ | Restraint Current in 87T |
| $I_{diff}^{h2}$ | 2nd harmonic of the differential current in 87T |
| $I_{diff}^{h4}$ | 4th harmonic of the differential current in 87T |
| $K$ | K index |
| $K_p$ | Planetary K index |
| $L$ | Observer Z state feedback signal gain |
| $L_b$ | Burden inductance |
| $L_{m,T}$ | Transformer magnetization branch inductance |
| $L_{m,CT}$ | CT magnetization branch inductance |
| $L_{p,T}$ | Transformer primary inductance |
| $L_{s,T}$ | Transformer secondary inductance |
| $L_{p,CT}$ | CT primary inductance |
| $L_{s,CT}$ | CT secondary inductance |
| $M2$ | 2nd harmonic set point for HR technique |
| $M4$ | 4th harmonic set point for HR technique |
| $N_i$ | Observer Z state gain |
| $R_b$ | Burden resistance |

| | |
|---|---|
| $R_{C,T}$ | Transformer core resistance |
| $R_{C,CT}$ | CT core resistance |
| $R_{p,T}$ | Transformer primary resistance |
| $R_{s,T}$ | Transformer secondary resistance |
| $R_{p,CT}$ | CT primary resistance |
| $R_{s,CT}$ | CT secondary resistance |
| $u(t)$ | State space model input signal |
| $X_e$ | Equilibrium point state vector |
| $x(t)$ | Vector of states in state space models |
| $y(t)$ | State space model output signal |

| | |
|---|---|
| $\beta$ | Ground Conductivity Coefficient used in NERC benchmarking |
| $\Phi$ | Magnetic Flux |
| $\lambda_{1,T}$ | Transformer primary flux |
| $\lambda_{2,T}$ | Transformer secondary flux |
| $\lambda_{m,T}$ | Transformer magnetization flux |
| $\lambda_{1,CT}$ | CT primary flux |
| $\lambda_{2,CT}$ | CT secondary flux |
| $\lambda_{m,CT}$ | CT magnetization flux |
| $\Theta$ | Latitude |
| $\Delta Long$ | Difference in longitude of two substation coordinates |
| $\Delta Lat$ | Difference in latitude of two substation coordinates |
| $\rho$ | Set of varying parameters for an LPV system |

*I dedicate this work to my parents.*

# Chapter 1

# Introduction

Geomagnetic Disturbances (GMDs) are a natural phenomenon that frequently occurs to the earth's magnetic shield and surface layers. They potentially can bring about various complications in man-made infrastructures such as railways, wired phone lines, radio communications and in particular in the power grid and its equipment [1].

In a power grid network, power transformers are critical elements with versatile uses such as power distribution for effective electrical energy transfer, Direct Current (DC) isolation and voltage regulation. The large size, price, and critical role of power transformers makes their maintenance an important task that requires careful deliberation; thus protection of transformers against damages is of great concern. It has been shown that GMDs can have negative impacts on power transformers operation and protection [2, 3]. This study in particular focuses on this issue and addresses its challenges.

In the following sections, first a brief explanation of the GMD phenomenon and its underlying process is provided to further familiarize the readers with origins of GMD and its process. This is then followed by a detailed description presenting how GMD leads to Geomagnetically Induced Currents (GICs) on the power grid and the harms it introduces to power transformers and their differential protection; giving out the notion of the problem investigated in this study. Afterwards, the literature review, research gaps, and objective are sequentially presented in the remaining of this chapter.

## 1.1 GMD Phenomenon: Background

GMDs are stemmed from the frequent interactions between solar storms and the magnetic shield of the earth, and their origins is attributed back to the interplay of matter in the Sun; where solar storm radiations are generated. In cases where the particles and

energy within the solar storms are directed towards earth, they make contact with it and interact with its outer surface, leading to creation of both electrical and magnetic variations in the upper layers of atmosphere. These in turn result in magnetic variations on the surface and give rise to GMDs [4–6].

Accordingly, comprehending the GMD phenomenon entails an understanding of the underlying aspects regarding solar storms and earth's outer atmosphere. In the following, these concepts that are primarily drawn from the planetary science field are explored.

The following first introduces the Sun's structure to locate the Corona layer, then it describes sunspots which are birthplace of solar storms. Next comes an explanation of the solar storms content, i.e. Coronal Mass Ejections (CMEs) and Co-rotating Interaction Regions (CIRs). Subsequently, for getting acquainted with frequency and temporal relation of severity of solar storms, the following brings up the solar cycle notion and a description of the earth's outer layers and magnetic field proceeds it. Having all of these information allows us to the unfold the GMD process.

### Sun structure and Sunspots

Sun is a giant star made of charged hot gases and plasma and it is mainly divided by an inner (core) and an outer layer. The outer layer is comprised of the several layers itself that includes Photosphere layer, Chromosphere layer, Transition region, and Corona layer as the outmost layer with no upper limit. Fig 1.1 [7, 8] (a) shows these layers. Corona layer is not easily visible and consists of plasma [7, 9, 10].

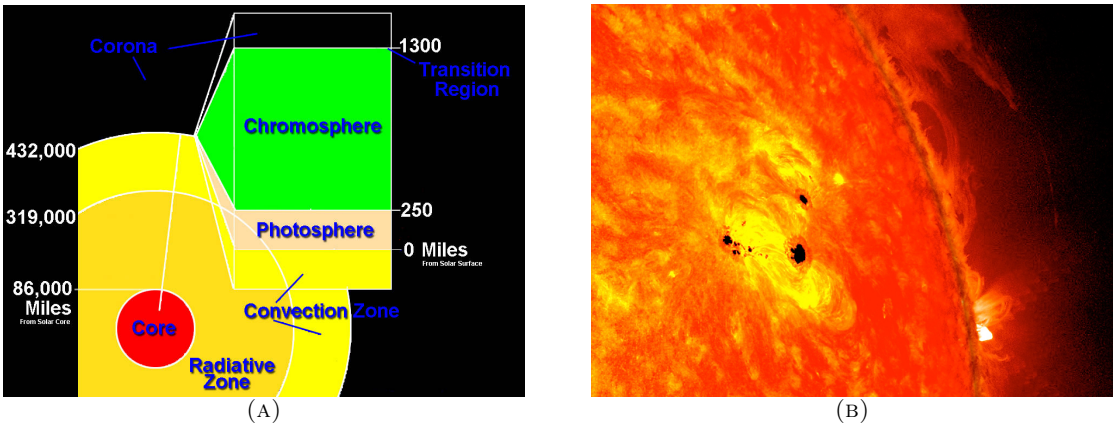


(A) (B)

FIGURE 1.1: A) Sun Layers B) Sunspots - credit: NASA [7, 8]

Spatio-temporal variations of matter reactions inside the sun cause intense magnetic fields to appear on the surface of sun, prohibiting heat inside the sun from reaching out to the surface. As a result, these areas take form of sunspots; dark regions where

temperature is lower than their surrounding. Fig. 1.1 (b) demonstrates sunspots as the dark regions on the surface of the Sun. [10, 11].

### Coronal Mass Ejections (CMEs) and Co-Rotating Interaction Regions (CIRs)

Outer layer of sun, Corona, is mostly made of very hot plasma and gases. These plasma material also contain magnetic fields, since plasma is a perfect conductive fluid and according to Alfven's frozen theorem, they carry the magnetic field with themselves. Often, bubbles of plasma and gas burst out of Corona layer which are called Coronal Mass Ejections (CMEs) [12, 13]. These CMEs may reach the earth two or three days after the bursting (when directed towards earth). Sunspots also can intensify these ejections. When magnetic field in the sunspot regions reconnect or reorganize, the stored energy of those magnetic fields discharges and it causes a huge release of energy, radiation bursts, typically in the form of heat, light, and electromagnetic energy (such as X-rays), and flares that accelerate the material on sun's Corona (mostly plasma), pushing them outward from sun into space [14]. Solar winds are streams of these CME particles with different speeds. When high speed CMEs (around 800km/s) interact with low speed (around 300km/s) ejections, they form co-rotating interaction regions (CIRs). Both CME and CIRs affect the earth, and they are both considered solar storms [8, 15]

### Solar Cycle

The interactions inside the sun lead to magnetic poles of sun being interchanged almost every 11 years, which affects the sunspot occurrences. During this 11-year period, there are times when sunspot incidents occur frequently (called Solar Maximum) and times when these activities are much lower and sun's surface is more quite (called Solar Minimum). Each solar cycle has one solar maximum and one solar minimum, as the historical recordings suggest. Severe solar storms can possibly occur at any time during the cycle, and solar minimum or maximum doesn't necessarily imply the severity. Nevertheless, CMEs are dominant during solar maximum and CIRs usually occur during solar minimum and the likelihood of GMD events are higher during solar maximum [16–18]. Fig. 1.2 [19] shows the recorded number of sunspots during solar cycle 23 to corroborate on the solar maxima and minima points.

### Earth Magnetic shield and Surface Layers:

Earth is a giant magnetic dipole. These magnetic field lines on the surface protect us against solar and cosmic radiations via deflection of particles and atoms; thus making

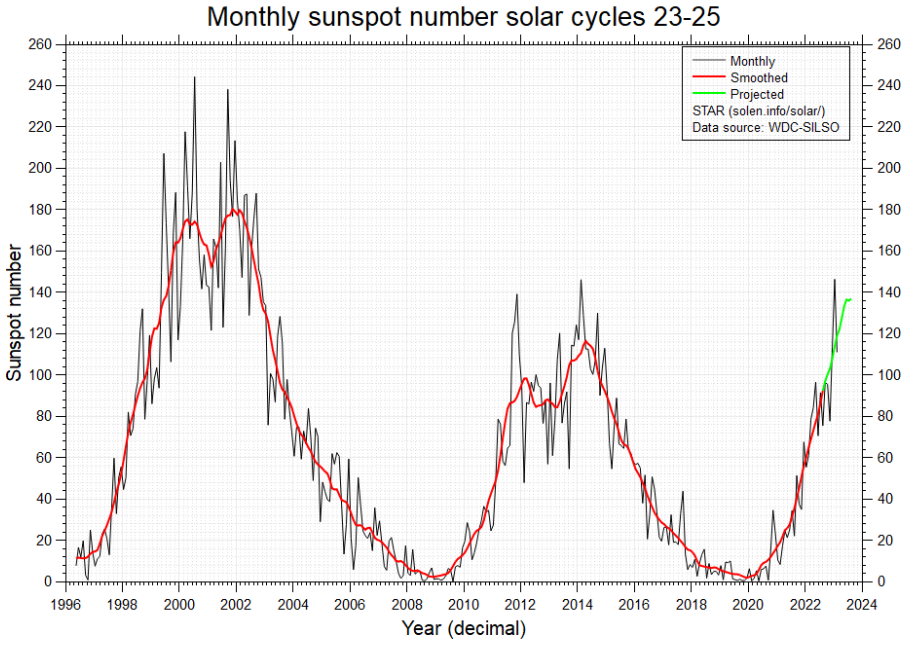


FIGURE 1.2: Solar maximum and minimum via sunspot numbers for solar cycle 23-25 [19]

earth habitable. Earth has an upward magnetic field, with N pole being located at the south of earth and S pole being located at north near arctic. The magnetic field area that covers surface of the earth is called Magnetosphere and it shown in Fig. 1.3 [20, 21] where white clouds represent the magnetic field lines. As can be seen in the figure, magnetosphere is compressed on the side of earth facing sun and is stretched on the night-side [20, 22].

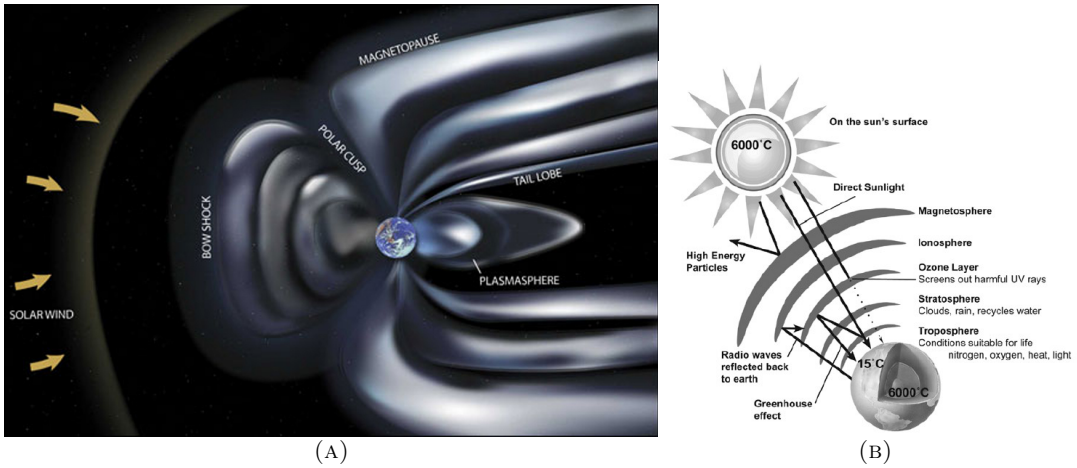


(A) (B)

FIGURE 1.3: (A) Magnetosphere; Magnetic shield of the Earth, (B) Atmospheric layers of Earth [20, 21]

Earth has several layers on its surface above the ground including the magnetosphere. Out of which, Ionosphere is of concern in this study. Ionosphere is located on earth's

atmosphere, roughly at 50 km to 965 km from the ground and is ionized, meaning that it is electrically conductive. Ionosphere has overlaps with magnetosphere, and has four layers named D, E, Es, and F. In layer E, there are Electro-Jets (huge electrical currents) carrying through [23].

## 1.2 GMD Process and GIC

As previously stated, GMD in broad terms is referred to as the outcome of interactions between solar storms and the magnetic shield of the earth, causing the magnetic field variations near the earth's surface. Nevertheless, there are additional details involved in the occurrence of GMD. More precisely, GMD is modelled with electric fields - or geo-electric fields in this context - relating to the variations in magnetic potential vector (A). Fig. 1.4 delineates chronically the events leading to a GMD and the way GICs are created as a result of GMD.

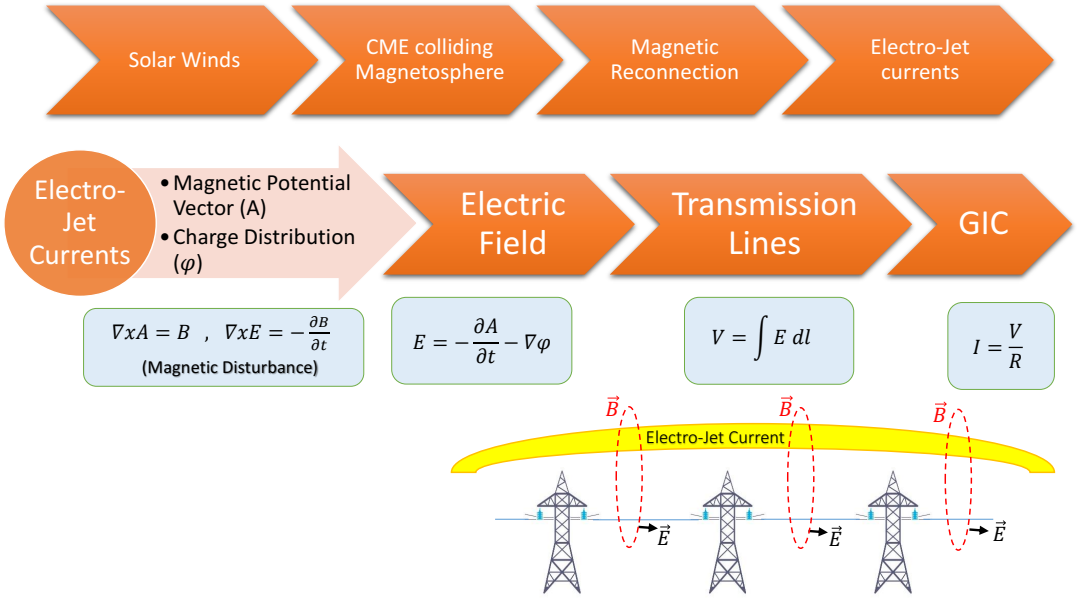


FIGURE 1.4: GMD process

As can be seen in the figure, solar radiation is the start of the process that leads to GMD phenomenon. When the solar storms are directed towards and hit earth, charged particles of its content or CMEs or CIRs collide with earth's magnetic shield (at day-side). While some of these particles are diverted by this shield, others can effectively enter the magnetosphere and transfer their energy onto earth via the neutral points created at the north and south magnetic poles. Neutral points are created by virtue of solar winds' downward magnetic field: magnetic reconnection of solar winds' downward field with earth's upward field occurs and neutral points on poles are created. The particles -which

carry electric charges- then move towards poles and branch off into spherical orbits in ionosphere, creating disturbing Electro-Jet currents in order of millions of amperes at the atmosphere, roughly 100 km above the surface [24] and also new charge distributions ($\Delta\Phi$). The currents induce magnetic fields along their flow rings, producing magnetic potential vectors (A). According to Faraday's law of induction, the varying A and $\Delta\Phi$ in turn produce geo-electric fields, which are considered as disturbances appeared on the surface. This extra geo-electric field induces voltage along long conductors (see Fig. 1.4) and where this voltages finds a closed loop path, current flows within that conductor. These currents flowing on conductors that are evolved from the GMD are called Geomagnetically Induced Currents (GICs) . Therefore, as a result of GMD, GICs are induced on man-made infrastructure, particularly on the ones with long conductors such as pipe lines, railways, and importantly power grid lines. [6, 15, 25].

## 1.3 GMD Duration and Metrics

This section briefly gives insight into the characteristics of GMD occurrences and quantifying methods for that, aiming to better familiarize reader with the phenomenon of GMD.

The GMD phenomenon may occur over a considerable amount of time that varies - it can be several hours or days. When describing temporal characteristic of a GMD event on earth, literature suggests that GMD goes through three phases [26]: initial, main (or maximum), and recovery (or decay). The initial phase (also called sudden storm commencement or SSC) takes few hours and the magnetic field on earth surface increases by some degree, then it changes from increasing to decreasing and main phase begins. At main phase, there is a sudden decrease in magnetic field, and then the recovery phase begins. Recovery can take several days, and usually for the GMDs related to high speed CMEs is one to two days and for the ones related to CIRs it can take many days [27].

There are a number of indexes suggested for measuring a GMD's severity. Indexes $Dst$, $K$, and $K_P$ are among those. $K$ index is the maximum magnetic fluctuations during 3 hours, and has a range from 0 to 9 with 0 meaning no fluctuations and 9 showing the highest fluctuations, meaning severe storm. When observed by several stations around the globe and averaged, the $K_P$ is formed, which is called the planetary K-index. Interestingly, $K$ and $K_P$ indexes can be expressed for other planets than earth as well. $Dst$ is the deviation from horizontal magnetic component over a period of one hour and is stated in unit of nT per hour. Recorded GMD events have shown $Dst$ ranges from -500 nT to several 1000 nT [15].

TABLE 1.1: $K_P$ index and its corresponding effects - NOAA [28]

| Kp | Descripted as | Avg Frequency (11 years) | On Power System |
|---|---|---|---|
| 9 | Extreme | 4 days per cycle | Voltage Control Problem<br>Protection Problem<br>Complete Collapse |
| 8 | Severe | 60 days per cycle | Voltage Control Problems<br>Protection Problems |
| 7 | Strong | 130 days per cycle | Voltage Correction<br>Protection False Alarm |
| 6 | Moderate | 360 days per cycle | Voltage Alarms<br>Transformer Damage |
| 5 | Minor | 900 days per cycle | Weak fluctuations in grid |

National Oceanic and Atmospheric Administration (NOAA) has provided a scale that maps an observed GMD with its $K_P$ index to possible effects on power systems. Table. 1.1 [28] shows parts of this scale that correspond to high $K_P$ indexes along with frequency of those storms occurring [28]. According to this, past storm incident recordings suggest that severe storms that can potentially lead to protection problems or transformer damage account for 13.8% of days in a solar cycle (11 years). Reports at [15] also suggest that storms with $K_P$ indexes of 7 and 8 account for most of the storms happened during solar cycles 23 and 24; corroborating on the possibility of strong storms in the future.

## 1.4 Effects of GMD on Power Grids and Transformers

A GMD manifests itself ultimately as GICs, flowing on power grid elements. As stated previously, GMD first prompts geo-electric field which induces considerable voltage on long conductors along it, i.e. power transmission lines in case of a power grid. When such lines are connected from both sides to ground, a return path through ground is provided, enabling the GIC to flow. In grounded $\mathrm{Y}-\Delta$ transformers, their neutral connections provide this closed path. Fig. 1.5 depicts the induced voltage corresponding to a GMD situation as $V_{DC}$, on transmission lines. This figure shows how GIC is formed as a result of the induced voltage and the closed path provided via two $\mathrm{Y}-\Delta$ transformers and the ground.

It is worth mentioning that It is not practical to avoid $\mathrm{Y}-\mathrm{Y}$ connections in a grid due to safety, technical, and protection issues.

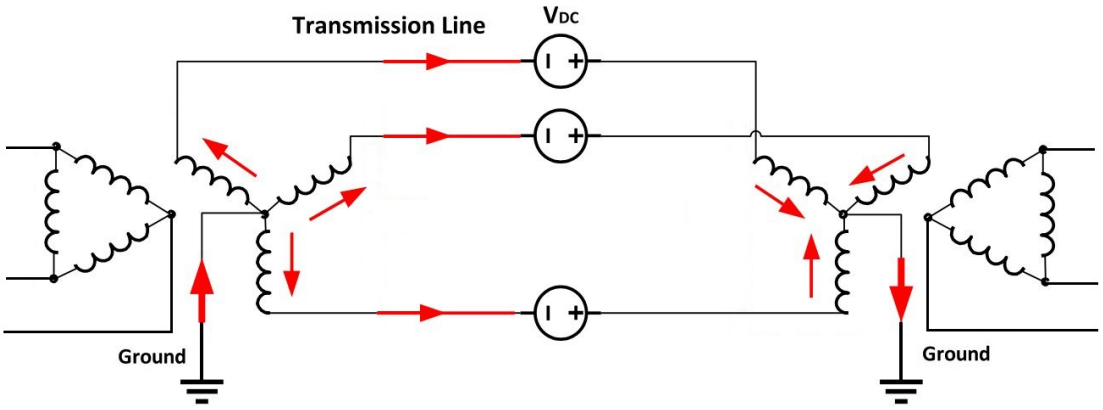


FIGURE 1.5: GIC closes its loop through YD transformers

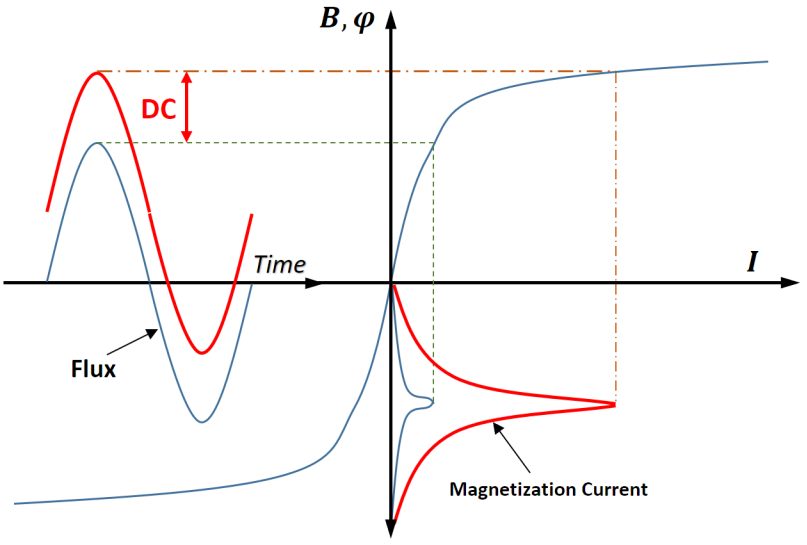


FIGURE 1.6: Effect of added DC flux on magnetization curve of transformer

GIC is a very slow varying current, with a frequency range of around 0.0001 Hz to 0.1 Hz. Compared to typical power grid frequencies (60 Hz or 50 Hz) its behavior can be viewed as a DC current component. Consequently, presence of GIC gradually adds up a DC component on power transformer currents - which are naturally AC waveforms. This in turn adds a DC flux to the magnetization flux of power transformers and their associated Current Transformers (CTs) [29]. This DC flux can saturate the cores of CTs and/or transformers. Fig. 1.6 shows how the added DC flux affects the magnetization currents, causing high magnitude peaks within the transformer or CT. Saturation of transformers and CTs leads to distorted current waves and elevated harmonic content in power transformers and onto other equipment of power grid such as generators and capacitor banks [15, 30, 31].

It has been shown that GICs can negatively impact the performance and operation of

power grids by either damaging or causing harm and disturbances to the equipment. Harmonics introduced due to GIC can cause capacitor banks trip out as they are susceptible to low impedance currents related to the harmonics. GIC DC current imposes excess heating on generator rotors and provoke vibration, possibly damaging or wearing mechanical parts. In the event of GIC, increased reactive power consumption occurs over the grid due to the Volt Ampere Reactive (VAR) consumption of transformers in the presence of DC components, which may even lead to black out if Static Var Compensators (SVCs) cannot respond to the excess demand. There are also chances that GMD events provoke communication losses. Global Positioning Systems (GPS) signals may be distracted over an area -which are essential for the power grid measurements [32] - and Power Line Carriers (PLC) may be unable to work properly [1, 33].

Due to the harmonics introduced by GICs, GMD events can potentially undermine operation of protection systems in power grids, e.g., by delaying the operation of distance relays or falsely tripping of generators [33, 34].

## 1.5 Transformer Differential Protection and Effect of GICs on It

There are many protection schemes to protect power elements in a power grid. Fuses, instantaneous over-current relays (element 50), time-delay over-current relays (element 51), and differential over-current relays (element 87T) are examples of such protective equipment. Transformers are often protected with differential protection relays due to their sensitivity and dependability, and the fact that input and output terminals of a transformer are geographically close [35].

Based on KCL law, in an ideal transformer, all the current entering the transformer (e.g., primary current for two-winding transformers) must flow out of it (through its secondary winding). The differential protection relay compares the entering and exiting currents through the element to find a difference between them. The existence of a difference indicates a fault occurred inside the transformer, and it is no longer working properly. Therefore, 87T relay along with a pair of circuit breakers can be used to trip out the transformer in case of a fault occurs [35]. Fig. 1.7 show a differential protection relay connected to a power transformer.

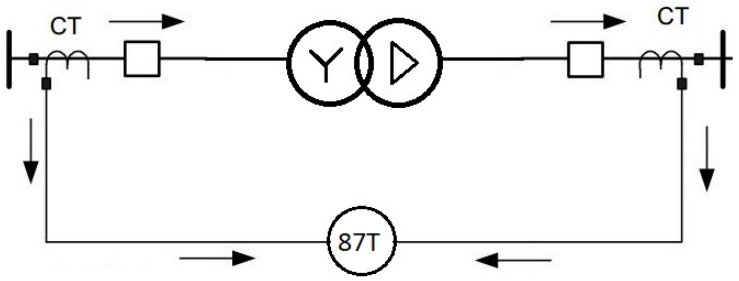


FIGURE 1.7: Transformer Differential Protection Relay and its connection to transformer

The working principle of a differential relay (87T) is as follows: First, differential current $I_{diff}$ and restraining current $I_{res}$ are calculated as below:

$$I_{diff} = \vec{I_p} + \vec{I_s} \tag{1.1}$$

$$I_{res} = |I_p| + |I_s| \tag{1.2}$$

In non-ideal transformers existence of losses and magnetization current initially imposes a difference between primary and secondary currents. Moreover, there are other situations for a healthy transformer that might add up to the calculated differential current in 87T. For instance, during energization of a transformer, inrush currents may be drawn from its primary winding due to existence of remnant flux in the transformer . Also, CTs used to scale-down transformer's currents for the differential relay may not exactly match with transformer's ratio in practice. Thus, marginal errors may be present that make $I_{diff}$ of a protective relay non-zero during normal operation. To address this issue, percentage differential relays are employed which have a margin of error for the differential current [35]. This margin of error is expressed by using a characteristic function $f_{87T}(I_{res})$. Fig. 1.8 shows an example of such a function, with a minimum pickup value and a ramp following it. The tripping logic for differential relays is therefore defined as:

$$I_{diff} > f_{87T}(I_{res}) \tag{1.3}$$

where $f_{87T}(.)$ provides a margin or error for any operating $I_{res}$, allowing for non-ideal transformers to be tripped out only when $I_{diff}$ is more than a certain threshold. Differential relays with above working principle are employed to protect power transformers in power grids.

Presence of GICs affects the performance of differential relays. The saturation of power transformers and CTs due to DC components of GIC can mislead the transformer differential element (i.e., 87T) into tripping the transformer [3]. As discussed in [36, 37], this

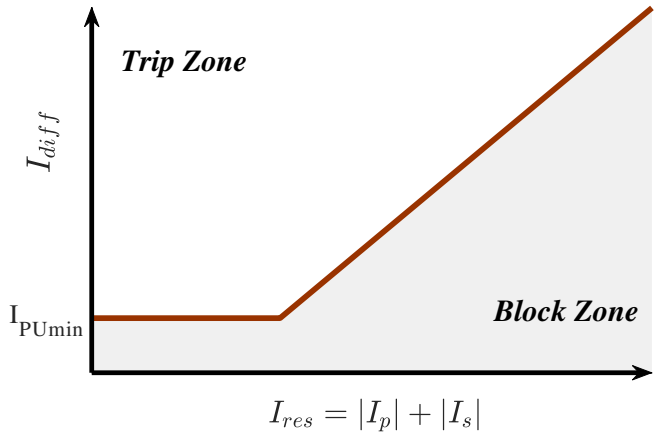


FIGURE 1.8: Basic 87T characteristic function

problem is more pronounced for single-phase transformers or three-phase transformer banks. To address this issue for 87T element, off-the-shelf commercial relays have been equipped with various functions, such as Harmonic Restrain (HR) and Harmonic Blocking (HB) [38, 39]. For instance, the relay in [38] utilizes the second, third, fourth, and fifth harmonics for blocking unwanted pickup of 87T element during CT/Transformer saturation, as well as during GMDs. This approach, however, disables the 87T element during GMDs—which often take a relatively long time to disappear [27]—to avoid its malfunction, thus leaving transformers unprotected. As a result, currently available transformer differential protection may not detect internal faults during GMDs [3, 40]. This problem has proven through detailed time-domain simulations in [41, 42]. Thus, there is an urge for developing a more-dependable/-secure differential protection scheme in the presence of GICs.

## 1.6 Literature Review

GMD phenomenon and its effects have been given extensive attention and there are various studies carried out on them. In this section, before delving into the effects of GMD, a brief history of the previous GMD events is forwarded to further enlighten the readers with the geographical and historical extent of this phenomenon and recorded damages regarding them. Afterwards, those of studies that correlate to the GMD phenomenon, its effects on power systems and transformers, and in particular the protection of transformers are given to bold the previous efforts on this topic. Moreover, efforts that are related to the challenges pertaining to the transformer differential protection under GIC has been given.

### 1.6.1 Historic GMD Events

Sun has an active surface; solar flares and cosmic radiations from sun are occurring every day and every moment. Historically, sunspots have been observed and recorded since 1600 and we are currently in the solar cycle 25 [43]. Copious historic GMD events have occurred in the past and some caused considerable damage to the man-made infrastructure. Carrington solar storm in 1859 is the largest storm that has ever been recorded, which caused failure of telegraph systems around Europe and USA [44]. In 1940, power system failure due to GMD has been observed in the USA and Canada [45]. Later, in March 1989, a GMD resulted in a total blackout in Québec, Canada, which impacted 6 million people, damaged two transformers, and imposed $6 billion in cost [46–48]. In October 2003, the Halloween Storm caused problems to high-voltage power systems of Sweden [49]. Moreover, in the past it was believed that GMD events have effects only on high-latitude northern countries. However, recently it has been observed that the GMDs can also impact lower latitude countries such as China and Brazil [50].

### 1.6.2 Effect of GIC on Power Transformers

There is a rich body of literature on the impacts of GMD on the behaviour of power transformers and CTs. In [51], it has been demonstrated through modeling and laboratory tests that CTs can saturate and their excitation current increases in the presence of GICs. Additionally, the impact of GIC on the excitation currents and harmonic behavior of single- and three-limb transformers is discussed in [37]. Reference [31] demonstrates that power transformers under GIC tend to highly increase their harmonic content with the increase of GIC magnitude. Moreover, it has been shown that although both odd and even harmonics are produced during GMDs, the second harmonic is a prominent indicator of GIC. Although these papers illustrate the nature and impacts of the GMD, they do not propose any solution for detecting and mitigating GICs.

### 1.6.3 GIC Detection

In order to detect GICs, both model- and Machine Learning (ML)-based approaches have been investigated in the literature. The authors of [52] propose a hybrid time-frequency analysis mixed with Convolutional Neural Networks (CNN) to detect GICs using CT measurements. In [53], a time-series of even harmonic measurements are used to train a CNN, which is implemented in a monitoring framework. Despite the acceptable performances of these ML-based techniques, they require abundant data for training, and their performance severely depends on the operating condition of the system. In

addition to ML-based techniques, another group of studies focus on developing GIC detection methods that rely on the mathematical model of the system. For instance, the authors of [54] convert CTs into fluxgate via current injection, and they measure DC currents of a transformer to detect GICs. This method, however, modifies the structure of CTs, which might not be desired in the industry. In [55], the extended Kalman filter is utilized to detect and estimate GICs. In this method, the nonlinearity of transformers' iron core is approximated by a two-term odd-order polynomial. This approximation, however, decreases the accuracy of estimation, and might result in erroneous protection decisions. By analyzing the reactive power absorbed by a power transformer, the authors of [36] estimate the GIC current flowing in a transformer. This method, nevertheless, only considers the fundamental frequency component, which might be inaccurate due to high levels of harmonics in the presence of GICs.

### 1.6.4 GIC Mitigation

In addition to above-mentioned studies, there are only a few research works focused on reducing the impacts of GMD on power grids. Some of these studies implement physical components, e.g., capacitors [56], magnetometers [57], and DC blocking filters at the neutral of transformers [58]. These methods, however, impose additional costs to the system, and might result in reliability and safety issues. Another group of studies, mitigate the impacts of GICs on 87T element by modifying its fault detection and tripping logic [38, 39]. As explained above, these methods negatively impact the security/dependability of differential relays during internal faults happening in the presence of GICs.

### 1.6.5 Transformer Protection under GIC

To the best of the authors' knowledge, there are only two studies, i.e., [42, 56], in the literature on the problem of protecting transformers against internal faults during GMDs. In [42], GICs and faults are detected and differentiated by monitoring the phase-angle of the second harmonic of differential currents and the rates of change of the fundamental component of differential currents, respectively. In [56], the three-phase instantaneous differential current waveforms are monitored and GICs are detected if all the waveforms are asymmetric in either a positive or negative direction. Using the rates of change of the fundamental component of differential currents, this paper also employs trip request signals for the relay unblocking purpose during GMDs. Although these two techniques are effective in general, they may result in the maloperation of 87T element when there is no internal fault, but the rates of change of the differential currents are

high during GMDs, e.g., when the CTs of differential scheme are severely saturated due to GICs.

## 1.7 Research Objective

To fill the above-mentioned gaps, this study shall make an effort to find methods to accurately detect transformer faults in the presence of GICs. In particular, this study aims to come with methods for single-phase transformers and three-phase transformer banks which are more susceptible to GIC. Additionally, this study is interested in methods that detect faults regardless of GIC presence, The key objectives that can distinguish the solution of this study from the existing methods in the literature are as follows: (i) it should be able to detect internal faults in the presence of GICs and CT saturation, (ii) it should negligibly affect the performance of 87T element in terms of its speed and sensitivity, (iii) it can be easily incorporated in commercial relays, (iv) it should not be dependent on the operating condition and parameters of power grids, and (v) it should not require abundant data for training and tuning.

## 1.8 Thesis outline

The rest of this thesis is organized as follows: the test system used in this study to elucidate the problem, and test the proposed solution is introduced in chapter two. After that, chapter three explores over the problem that is addressed in this study by examining simulation results for the mentioned test system. Two coming next chapters delve into the proposed solution of this study. Chapter four furnishes models that the proposed framework requires. Specifically, it provides a state-space model of power transformers and CTs, and introduces an observer model for them. Having these requirements, chapter five describes the proposed framework and elaborates on the two schemes used in it. Chapter six evaluates the performance of the proposed framework through different scenarios designed based on the given problem. This chapter verifies the ability of the framework to detect faults under GIC. Conclusion and future work are given in chapter seven.

# Chapter 2

# Test System

This study utilizes a modified version of the IEEE 118-bus test system sketched from U.S. Midwest power grid [59] for simulating the problem and verifying the proposed solution. The modifications to this test case are adopted from [60], and applied in Electromagnetic Transient Program (EMTP) software. The test system has 118 buses operating at voltage levels of 120 and 315 kV. All 117 transmission lines of this test system are presented by their equivalent $\pi$ models. There are 69 generators in 20 power plants, 34 synchronous condensers, and 91 loads, all of which interfaced with the network via Y$-\Delta$ banks of transformer. Additionally, there are nine Y$-$Y banks of transformers that interface transmission lines. Figure 2.1 shows the single line diagram of this test system.

Given that GMDs mainly effect Y$-\Delta$ transformers with grounded neutral, which provide a close path for circulation of GICs, load and generator transformers are dominantly affected during this phenomenon. As a result, without loss of generality, this study focuses on the 138 kV/25 kV 44 MVA Y$-\Delta$ load transformer at Bus 46 (i.e., T46), and studies the behaviour of this transformer during GMDs. The reason for focusing on this transformer is that it experiences more-severe GICs, and thus it shows the problem more clearly. This transformer feeds a load consuming 28 MW of active and 10 MVAr of reactive power. To model this transformer and its associated differential protection scheme accurately, the non-linear flux-current characteristics shown in Figs. 2.2 (a)-(c) are used for simulating T46 and its CTs (i.e., $CT_1$ and $CT_2$). Additionally, the parameters of the CTs are presented in Table 2.1. The 87T element protecting T46 is set based on the default settings of [39], and its dual-slope characteristic (i.e., $f_{87T}(I_{res})$) is shown in Fig. 2.2 (d).

For simulations, GICs are modeled based on the guidelines provided by the North American Electric Reliability Corporation (NERC) [24]. According to these guidelines, the

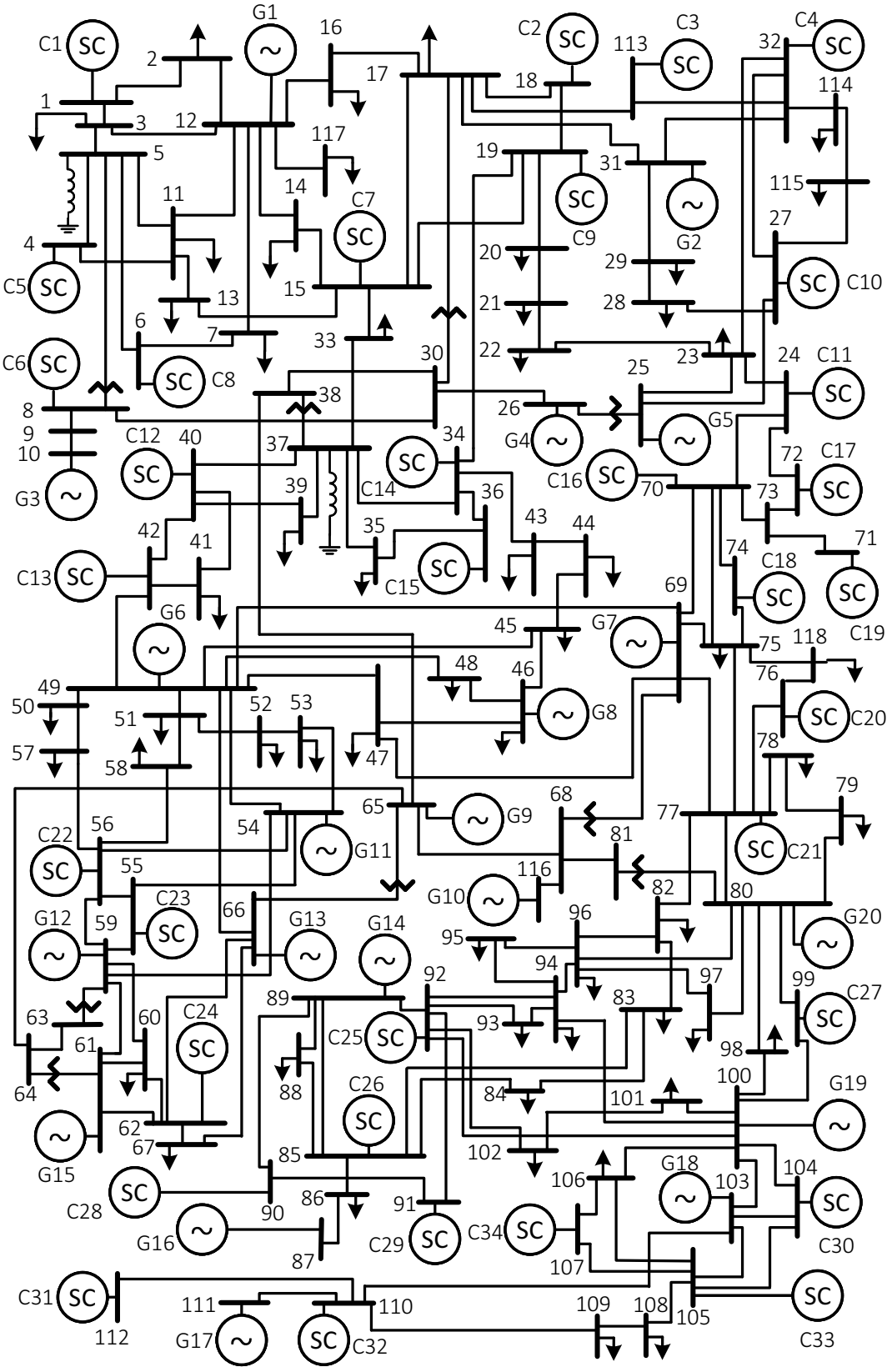


FIGURE 2.1: Modified IEEE 118-bus test system.

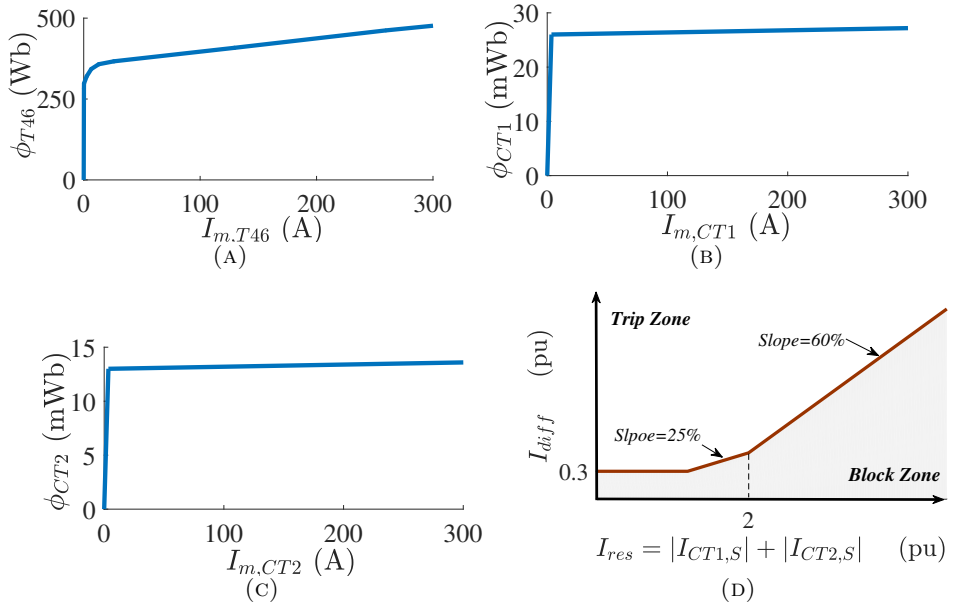


FIGURE 2.2: Magnetization curves of (A) T46, (B) $CT_1$, and (C) $CT_2$, as well as (D) 87T characteristic used for T46.

TABLE 2.1: Specifications of CTs used for protecting T46.

| Parameters | CT | |
|---|---|---|
| | 1 | 2 |
| Accuracy class | C400 | C400 |
| Turn ratio | 250:5 | 800:5 |
| Tap | 1.0 | 1.0 |
| Rated power (VA) | 500 | 500 |
| Rated frequency (Hz) | 60 | 60 |
| Core Resistance ($\Omega$) | 400 | 500 |
| Burden ($\Omega$) | 20.0 | 20.0 |
| Power factor of the burden | 0.9 | 0.9 |
| Primary resistance ($\mu\Omega$) | 1.2 | 3.1 |
| Primary leakage inductance ($\mu$H) | 0.0042 | 10.6 |
| Secondary resistance ($\Omega$) | 0.15 | 0.31 |
| Secondary leakage inductance ($mH$) | 0.53 | 1.06 |

effects of GMDs are modeled by DC voltage sources placed in series with transmission lines. These sources result in GICs flowing in the lines when there is a closed path for currents (e.g., in lines surrounded with Y–$\Delta$ transformers at both sides). To model these DC sources, a GMD benchmark, which contains the recordings of the GMD event that happened on March 1989 and resulted in Hydro Quebec blackout [61], is utilized. This benchmark provides the Geoelectric Fields (GEFs) produced by variations of GMD-driven magnetic field (i.e., $\frac{\partial \beta}{\partial t}$) near earth surface.

Using the recorded GEFs, the induced DC voltage alongside each transmission line can be calculated using the following equation:

$$V_{GMD,i} = \int \vec{E}_i . \vec{dl}_i \tag{2.1}$$

where $V_{GMD,i}$ is the DC voltage induced on transmission line $i$, $\vec{E}_i$ is the GEF around

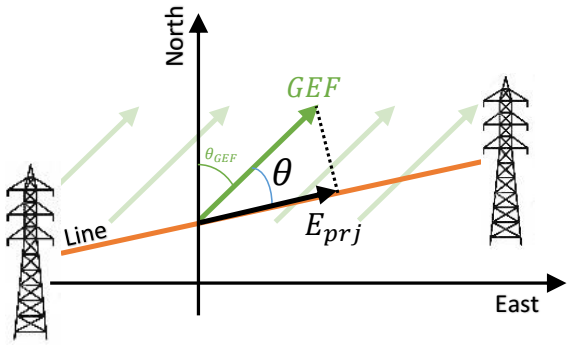


FIGURE 2.3: *GEF* on the area has an effective intestity that is found by calculating the projected value

transmission line $i$, and $\overrightarrow{dl}_i$ is the differential element of length along line $i$. It is commonly assumed in GMD studies that the projected element of $\overrightarrow{E}_i$ on line $i$ is constant over the length of the line and does not change significantly for short, medium, and large transmission lines [60]. Thus, (2.1) can be simplified to

$$V_{GMD,i} = E_{prj,i} L_i \tag{2.2}$$

where $L_i$ is the length of transmission line $i$, and $E_{prj,i}$ is the projection of $\overrightarrow{E}_i$ on this line, which can be calculated using the following equation

$$E_{prj,i} = \mid \overrightarrow{E}_i(GEF, \Theta) \mid \cos(\theta) \tag{2.3}$$

where $\theta$ is the angle between the GEF vector and the line, calculated using the direction of $\overrightarrow{E}_i$ and the coordinates of the line and $\Theta$ is the latitude corresponding to that transmission line (see Fig. 2.3).

$\overrightarrow{E}_i(GEF, \Theta)$ for each transmission line is eventually derived from the recommendations of NERC using a reference $GEF$ vector with two magnitudes of 4 V/km and 10 V/km, and an angle of 35ith the prime meridian, recorded at the latitude of 60° N. The reference magnitude recorded in NERC is particularly set for that certain latitude, and that's why the value of $\overrightarrow{E}_i(GEF, \Theta)$ for each line $i$ depends on the latitude of line. The $\overrightarrow{E}_i(GEF, \Theta)$ has to be calculated from the reference magnitude via scaling that reference value at 60° N latitude to other latitudes where each transmission line is installed.

Following shows how $\overrightarrow{E}_i(GEF, \Theta)$ is obtained via scaling from the recorded reference. Based on the benchmark, GEF is assumed to be a field vector with an angle and an amplitude over a certain area, with values recorded at a certain latitude. This GEF then scales to other areas as the following [62]:

TABLE 2.2: Parameters used for GMD simulations in this study

| $GEF_{mag}$ | GEF Angle | $\beta$ | Set Lat |
|---|---|---|---|
| 10 V/km | 35° | 1.0 | 60° |
| 4 V/km | 35° | 1.0 | 60° |

$$\overrightarrow{E}_i(GEF, \Theta) = \beta.GEF_{mag}.\alpha(\Theta) \tag{2.4}$$

Where $\beta$ is a factor representing the earth conductivity and is determined by the geological region table available via NERC benchmarking in [61], $GEF_{mag}$ is the magnitude of the GEF and is given $10V/km$ and $4V/km$ based on the benchmark recording, and $\alpha(\Theta)$ scales the GEF for that recording at local geomagnetic latitudes by:

$$\alpha(\Theta) = 0.001 \times e^{0.115 \times \Theta} \tag{2.5}$$

The given $\overrightarrow{E}_i(GEF, \Theta)$ from Eq 2.4 is then applicable to each of the transmission lines existing on the grid.

$L_i$ required for Eq 2.2 - which is the length of transmission line - can be obtained by calculating the GPS coordinates of the substations from [60] as following:

$$L_i = \sqrt{l_x^2 + l_y^2} \tag{2.6}$$

Where:

$$\begin{cases} l_x = 111.2 * \Delta Long \\ l_y = 111.2 * \Delta Lat * \sin\left(\frac{\pi}{2} - \frac{\Delta Long}{2}\right) \end{cases}$$

where $\Delta Long$ is the longitude difference of the start and end for the substations of transmission line $i$ and $\Delta Lat$ is the latitude difference of those. Plugging in the coordinates and projected GEF magnitude, $V_{GMD,i}$ voltage source is determined for each of the transmission lines.

Summary of the set values based on the NERC benchmarking that have been used for the simulation in this study are given in the Table 2.2.

It should be noted that $\beta = 1.0$ is the value relating to Ontario and Quebec region, according to the NERC benchmarking. This $\beta$ value corresponds to the GEF recordings in the benchmark, which is related to the Hydro-Quebec event.

More information about calculating $\overrightarrow{E}_i$ around each transmission line based on the reference GEF vector can be found in [62].

# Chapter 3

# Problem Statement

As explained in chapter 1, the majority of off-the-shelf differential relays employ an HB and/or HR module to prevent maloperation of 87T element in the presence of high-harmonic currents. Such currents can be generated due to part-cycle saturation of transformers during GMDs. Thus, the majority of commercial relays block 87T element during GMDs, which often take long (e.g., several hours or a day [27]) to disappear. As a result, as this chapter proves, the operation of 87T element is also blocked for in-zone short-circuit faults that might happen during severe GMDs, resulting in potential irreversible damages to transformers.

In simulations, the GMD phenomenon (the magnitude of the reference GEF is 10 V/km) starts at $t = 0$, and $V_{GMD,i}$ is induced on transmission lines. As a result, wherever there is a closed path for GICs, the DC component of currents passing through CTs and transformers increase exponentially. The resultant DC current generates a DC flux in the cores of CTs and might shift their operating point into the saturation zone. The same phenomenon happens in power transformers, but with a slower pace due to their larger $L/R$ ratio. Figs. 3.1 and 3.2 show the core flux ($\phi$) and magnetization current ($I_m$) of T46 and CT1 during the GMD. The DC flux generated by GICs increases the half-cycle magnetization current of CTs and the transformer, resulting in distortion of their secondary currents. Fig. 3.3 shows the secondary currents of CT1 and T46 (i.e., $I_{s,CT1}$ and $I_{s,T46}$, respectively), as well as their primary currents transferred to the secondary side (i.e., $\frac{I_{p,CT1}}{n_{CT1}}$ and $\frac{I_{p,T46}}{n_{T46}}$, respectively). As this figure shows, CT1 is severely saturated in 100 ms after the initiation of the GMD, while T46 needs a longer time to get severely saturated (it enters the saturation region 1.2 seconds after the GMD starts). In this process, the DC current of the transformer builds up initially with a lower pace, due to its larger $L/R$ ratio, and afterwards with a higher one, when the operating point enters the saturation region. Distortion of the secondary currents of

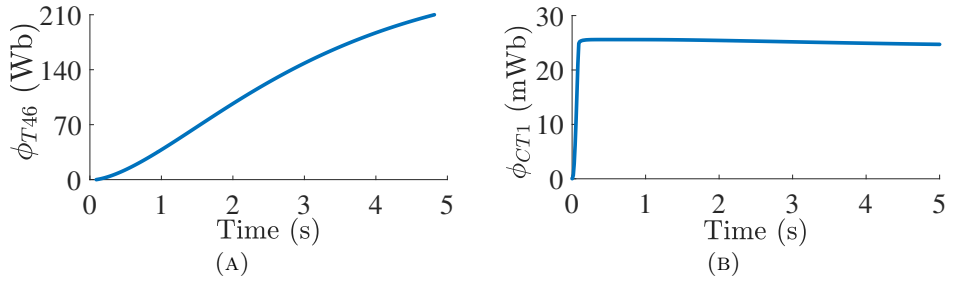


FIGURE 3.1: DC flux rise of (a) T46, and (b) CT1 during the simulated GMD phenomenon.

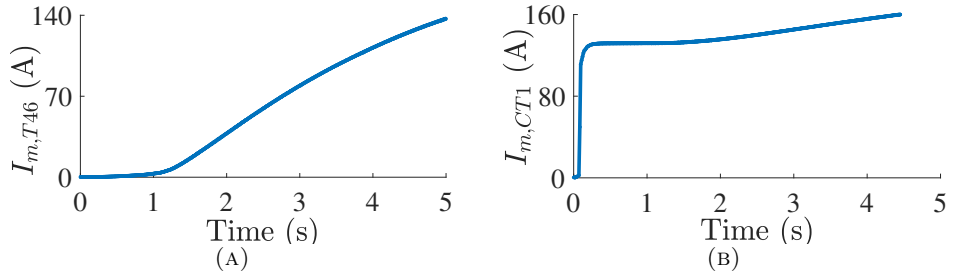


FIGURE 3.2: Magnetization current of (a) T46, and (b) CT1 during the simulated GMD phenomenon.

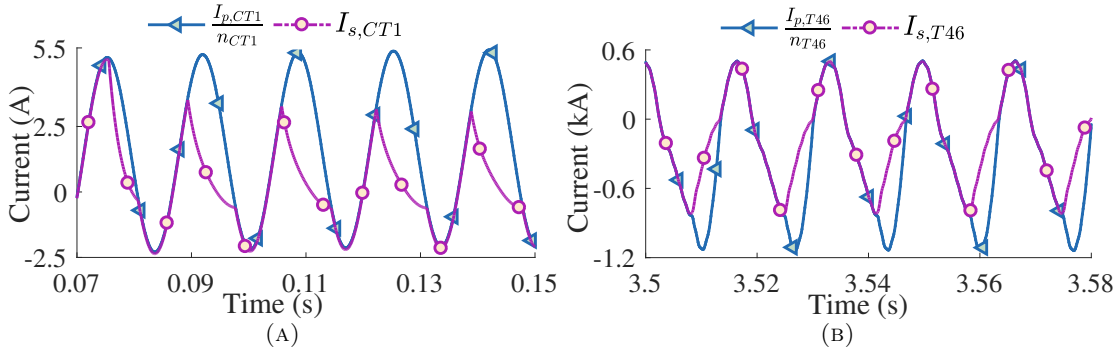


FIGURE 3.3: Secondary current waveforms of A) CT1 and B) T46 during the simulated GMD.

CTs and transformer results in inaccurate current measurements, potentially leading to maloperation of 87T element. To further investigate the impact of GMD on transformer differential protection, in the rest of this section, it is assumed that CTs are ideal and are not affected by GICs. Later on, this assumption will be revisited and corrective techniques will be applied.

Fig. 3.4 shows the operating point of 87T element before the GMD starts, as well as the relay's trajectory during the GMD. The increased magnetization current of the transformer rises $I_{diff}$ and $I_{res}$ and the trajectory enters the tripping zone. As a result the relay falsely trips the transformer if no corrective technique is in place. However, as mentioned in Chapter 1, to address this problem modern differential relays utilize HR or HB techniques to avoid malfunctioning of 87T element during transformer saturation

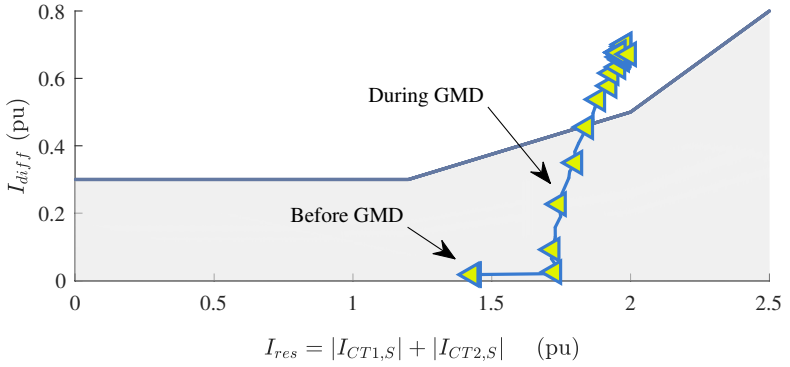


FIGURE 3.4: Trajectory of 87T element during the simulated GMD.

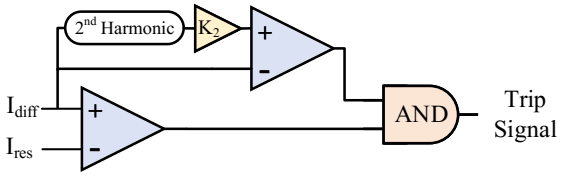


FIGURE 3.5: Harmonic blocking technique used by modern relays.

in general, and GMDs in particular. HB method effectively blocks the tripping signal of the relay when the harmonic content of the differential current goes beyond a certain threshold (e.g., 20% [63]). Fig. 3.5 shows the block diagram of the HB technique. Relays with HR method, however, use a modified characteristic to add extra restraint to the relay's operation during saturation conditions and detect faults if

$$I_{diff} \geq \underbrace{f_{87T}(I_{res}) + \frac{I_{diff}^{h2}}{M_{2h}} + \frac{I_{diff}^{h4}}{M_{4h}}}_{I_{res,h}} \tag{3.1}$$

where $M_{2h}$ and $M_{4h}$ are the set points for 2nd-harmonic and 4th-harmonic blocking, respectively, and are both set to 20% [63]; $I_{diff}^{h2}$ and $I_{diff}^{h4}$ are the second and fourth harmonics, respectively; and $f_{87T}(I_{res})$ is the characteristic of the conventional 87T element, which is shown in Fig. 2.2 (d). As Figs. 3.6 and 3.7 show, both methods effectively avoid false tripping of the transformer during the simulated GMD, and the transformer is not falsely tripped.

Although HR and HB techniques both can successfully avoid unwanted tripping of transformers during GMDs, they might avoid tripping of the transformer if an internal fault happens concurrently with the GMD (Figs. 3.8 and 3.9). Such faults are not unlikely considering the long duration of GMDs, as well as overheating of the transformer as a result of elevated excitation currents and stray flux closing outside of the transformer magnetic core [14, 27]. As Fig. 3.8 shows, when an internal 15% Turn-to-Turn (TT) fault happens in the presence of GICs, the HB method blocks the tripping signal of the

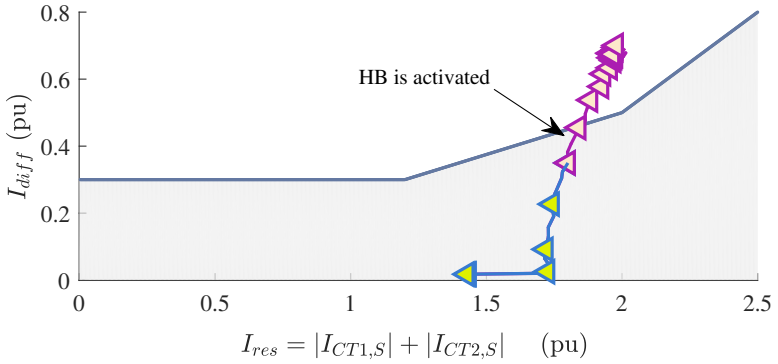


FIGURE 3.6: Trajectory of the differential relay equipped with the HB technique during the simulated GMD.

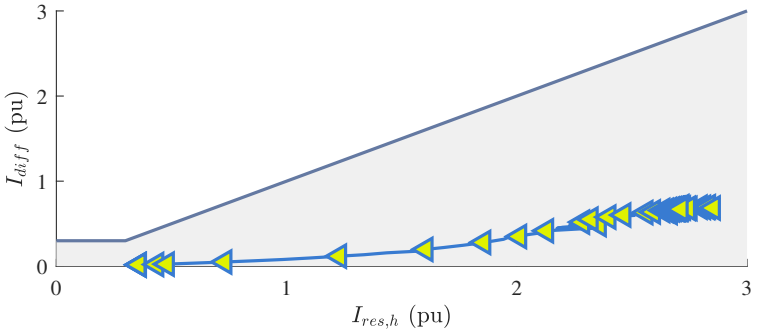


FIGURE 3.7: Trajectory of the differential relay equipped with the HR technique during the simulated GMD.

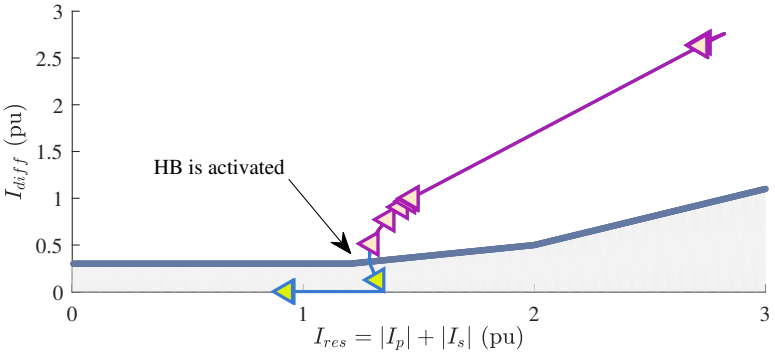


FIGURE 3.8: Trajectory of the differential relay equipped with the HB technique during the simulated internal fault and GMD.

87T element due to the high harmonic content of the differential current, so the internal faults remain uncleared. Similarly, as Fig. 3.9 shows, the HR module also prevents clearance of the internal fault by adding extra restraint. This issue and the resultant high fault current can lead to potential irreversible damages to the transformer.

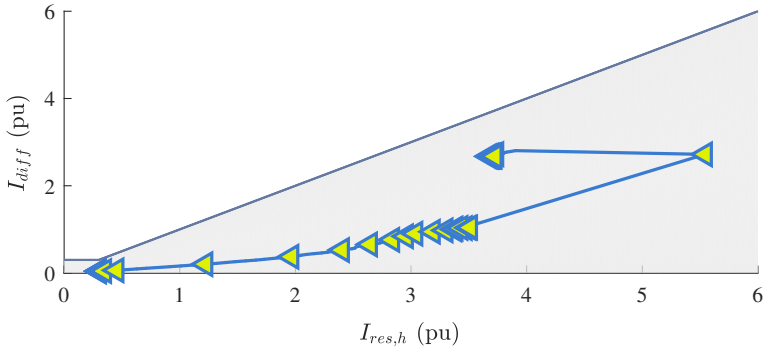


FIGURE 3.9: Trajectory of the differential relay equipped with the HR technique during the simulated internal fault and GMD.

As shown in this chapter, GICs add DC components to the magnetization flux of transformers, shifting their working points into saturation regions. Large magnetization currents of saturated transformers could possibly cause $87T$ to pick up. However, HR and HB techniques successfully avoid this and keep the transformers in the grid, as this chapter's simulations corroborate. Nevertheless, as can be seen through the results of this chapter, if a fault happens when GICs exist, 87T does not trip out the transformer. The subsequent chapters propose an auxiliary framework to address this issue.

# Chapter 4

# Modelling and State Estimation for Transformers

This chapter delivers models that are used by the proposed auxiliary framework on the protection relay in the next chapter. Currently, transformer differential protection relays make use of instantaneous current magnitude and angle for calculation and decision making in protective purposes. To adjust for the inherent non-ideal aspects of a transformer that may lead to maloperation of relay, they incorporate error margins and harmonic methods such as harmonic blocking or harmonic restraining [40]. This implies that harnessing a precise model of transformer - which is less prone to exhibit incorrect values - can help the relays in avoiding maloperation via removing the need to compensate for incorrect values. Considering that an accurate representative model of transformers benefits the decision making process inside protective relays, accurate transformer and CT models are developed here.

Transformers and CTs are dynamic systems that operate based on physical and electrical laws. Modelling dynamic systems can be done via analytical or experimental (data-driven) approaches. Data-driven approaches require model data to train or form a function that can describe behavior of the system and they may contain parameters that doesn't have a physical meaning or a concise relation to the physical aspect of the system. Analytical approaches on the other hand don't need experimental data; they exploit physical and mathematical laws to describe the model. Moreover, parameters in those models bear information regarding physical elements within the dynamic system that is being modelled [64]. Considering (a) the solidity and reliability of analytical approaches when they are available, and (b) the unfavorable demand of experimental data in data-driven models, this study uses an analytical approach to model transformers and CTs.

State space representation of dynamic systems is a powerful technique for providing functions that can best describe a system's model. It allows for accurate implementation of non-linear function compared to the linear methods such as single-input single-output transfer functions and it relies on time-domain methods, contrary to frequency-domain approach in classic linear methods [65]. Thus, transformer and CT models are going to be presented in state space domain.

Generally, state space models define a relationship between input (or inputs), system states, and output (or outputs) as follows:

$$\begin{cases} \dot{x}(t) = f(x(t), u(t)) \\ y(t) = g(x(t), u(t)) \end{cases} \tag{4.1}$$

Above form for Time-Varying systems changes to:

$$\begin{cases} \dot{x}(t) = A(t)x(t) + B(t)u(t) \\ y(t) = C(t)x(t) + D(t)u(t) \end{cases} \tag{4.2}$$

where $x$ is the the vector of states, $u$ is the input and $y$ shows the output. Term $D$ denotes the direct relation between input and output which is often zero. According to [64], although there exists a minimum number of states to represent the output for any given set of states $x(t)$ in a unique way, it is possible to have more than that.

## 4.1 Linear Parameter Varying (LPV) systems and Polytopic Form

LPV systems are those systems that have only constant or linearly varying elements in their $A$ or $B$ matrices. Consider below definition for an LPV system:

$$\begin{cases} \dot{x}(t) = A(\rho)x(t) + B(\rho)u(t) \\ y(t) = Cx(t) \end{cases} \tag{4.3}$$

In the above, $\rho$ is the set of parameters that vary, e.g. $\rho = \{\varrho_1, \varrho_2, \ldots, \varrho_m\}$, and $A$ and $B$ matrices are a function of those parameters. An example of a varying matrix for $A$ is given below:

$$A = \begin{bmatrix} 3 & \varrho_1 \\ 1 & \varrho_2 \end{bmatrix} \tag{4.4}$$

where $\varrho_1$ and $\varrho_2$ can each take a scalar number, and they can be a function of time.

In matrices $A$ or $B$, when $\rho$ parameters vary on a closed interval, for each of varying elements $i$, they can be decomposed to a lower and upper bound element along with coefficients $\mu_{i,1}$ and $\mu_{i,2}$ to reconstruct the original varying matrix, with $\mu_{i,1} + \mu_{i,2} = 1$. Consider the example above of $A$. Assume $\varrho_1 \in [1, 5]$ and $\varrho_2 \in [-1, 3]$. Then, matrix $A$ can be decomposed to:

$$A = \mu_{1,1} \underbrace{\begin{bmatrix} 3 & 1 \\ 1 & 0 \end{bmatrix}}_{A_{1,1}} + \mu_{1,2} \underbrace{\begin{bmatrix} 3 & 5 \\ 1 & 0 \end{bmatrix}}_{A_{1,2}} + \mu_{2,1} \underbrace{\begin{bmatrix} 3 & 0 \\ 1 & -1 \end{bmatrix}}_{A_{2,1}} + \mu_{2,2} \underbrace{\begin{bmatrix} 3 & 0 \\ 1 & 3 \end{bmatrix}}_{A_{2,2}} \tag{4.5}$$

where $A_{1,1}$ and $A_{1,2}$ are the lower and upper matrices for varying element $\varrho_1$ and $A_{2,1}$ and $A_{2,2}$ are the lower and upper matrices for varying element $\varrho_2$. Polytopic form of $A(\rho)$ therefore can be constructed as:

$$A = \sum_{i=1,j=1}^{i=2,j=2} \mu_{i,j} A_{i,j} \tag{4.6}$$

Moreover, $j$ can be embedded inside the $i$ items. Similar to the above technique, LPV systems can be expressed in Polytopic forms as below:

$$\begin{cases} \dot{x}(t) = \sum_{i=1}^{m} \mu_i (A_i x(t) + B_i u(t)) \\ y(t) = Cx(t) \end{cases} \tag{4.7}$$

In the following sections, first the state-space model of a single-phase transformer is developed. Same model can be applied individually for single transformers in a three-phase transformer bank. Afterwards, next section modifies the obtained model to adapt it for CTs by inserting the CT burden circuit. This CT burden contains a resistive-inductive load. Section 4.4 then uses the state space models of CTs and transformers to design observers for estimating their states. These estimated states will be used in the auxiliary framework introduced at chapter 5 to tackle the maloperation of 87T element when an internal fault happens during a GMD.

## 4.2 State Space Model of Transformers

The equivalent circuit of a transformer—in which all secondary parameters are transferred to the primary side—is used as shown in Fig. 4.1. In this circuit, subscripts $T$, $p$, and $s$ denote the transformer, its primary winding, and its secondary winding,

respectively; $n$ is the turn ratio; $V$ and $I$ represent the voltages and currents of the transformer; $R$ and $L$ signify the resistance and leakage inductance of windings; and $R_c$ and $L_m$, respectively, represent core losses and the non-linear magnetization inductance, which are both modeled at the primary side. The value of $L_m$ depends on the core magnetization flux, i.e., $\lambda_m$, and can be determined from the transformer's excitation curve—which can be obtained in an excitation test—for any flux value [66] [67].

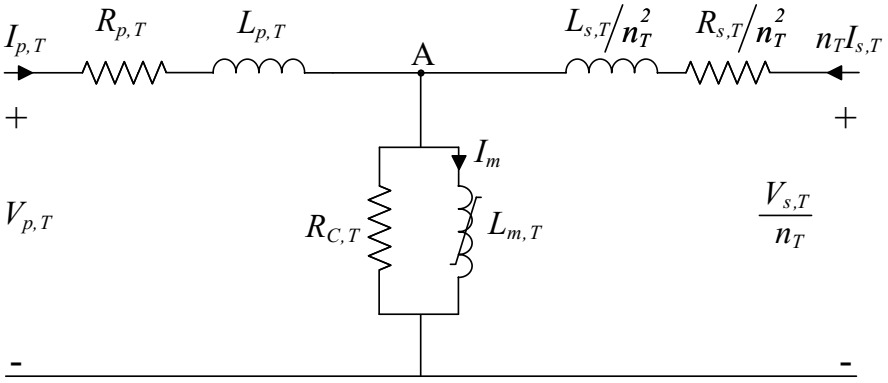


FIGURE 4.1: Equivalent circuit of Transformers.

By defining $\lambda_m$ as the core magnetization flux, $\lambda_1$ as the sum of the leakage flux of the primary winding and the magnetization flux, and $\lambda_2$ as the sum of the leakage flux of the secondary winding and the magnetization flux, the primary, secondary, and magnetization currents can be written as

$$I_p = \frac{\lambda_1 - \lambda_m}{L_p} \tag{4.8}$$

$$I_s = n\frac{\lambda_2 - \lambda_m}{L_s} \tag{4.9}$$

$$I_m = \frac{\lambda_m}{L_m(\lambda_m)} \tag{4.10}$$

Using (4.8) and (4.9), writing KVL equations for left- and right-hand-side meshes result in

$$\frac{d\lambda_1}{dt} = -\frac{R_p}{L_p}\lambda_1 + \frac{R_p}{L_p}\lambda_m + V_p \tag{4.11}$$

$$\frac{d\lambda_2}{dt} = -\frac{R_s}{L_s}\lambda_2 + \frac{R_s}{L_s}\lambda_m + \frac{V_s}{n} \tag{4.12}$$

Additionally, substituting $I_p$ and $I_s$ from (4.8) and (4.9) into the equation that is obtained by combining the KVL equation of the middle mesh and KCL equation at node A yields

$$\frac{d\lambda_m}{dt} = \frac{R_c}{L_p}\lambda_1 + \frac{n^2 R_c}{L_s}\lambda_2 - R_c(\frac{1}{L_p} + \frac{n^2}{L_s} + \frac{1}{L_m})\lambda_m \tag{4.13}$$

By modeling the primary and secondary voltages (i.e., $V_{p,T}$ and $V_{s,T}$) as inputs and the secondary current ($I_{s,T}$) as the output, (4.11)-(4.13) can be written in the following state-space form:

$$\begin{cases} \underbrace{\begin{bmatrix} \dot{\lambda}_{1,T} \\ \dot{\lambda}_{2,T} \\ \dot{\lambda}_{m,T} \end{bmatrix}}_{\dot{x}_T(t)} = \underbrace{\begin{bmatrix} -\frac{R_{p,T}}{L_{p,T}} & 0 & \frac{R_{p,T}}{L_{p,T}} \\ 0 & -\frac{R_{s,T}}{L_{s,T}} & \frac{R_{s,T}}{L_{s,T}} \\ \frac{R_{c,T}}{L_{p,T}} & \frac{n_T^2 R_{c,T}}{L_{s,T}} & \theta_T(\lambda_{m,T}) \end{bmatrix}}_{A_T} \underbrace{\begin{bmatrix} \lambda_{1,T} \\ \lambda_{2,T} \\ \lambda_{m,T} \end{bmatrix}}_{x_T(t)} + \underbrace{\begin{bmatrix} 1 & 0 \\ 0 & \frac{1}{n} \\ 0 & 0 \end{bmatrix}}_{B_T} \underbrace{\begin{bmatrix} V_{p,T} \\ V_{s,T} \end{bmatrix}}_{u_T(t)} \\ \underbrace{I_{s,T}}_{y_T(t)} = \underbrace{\begin{bmatrix} 0 & \frac{n_T^2}{L_{s,T}} & \frac{-n_T^2}{L_{s,T}} \end{bmatrix}}_{C_T} \underbrace{\begin{bmatrix} \lambda_{1,T} \\ \lambda_{2,T} \\ \lambda_{m,T} \end{bmatrix}}_{x_T(t)} \end{cases} \tag{4.14}$$

where $\theta(.)$ is defined as follows:

$$\theta_T(\lambda_{m,T}) = -R_{c,T}\left(\frac{1}{L_{p,T}} + \frac{n_T^2}{L_{s,T}} + \frac{1}{L_{m,T}(\lambda_{m,T})}\right) \tag{4.15}$$

In the above state-space equation, $L_{m,T}(\lambda_{m,T})$ is a function of magnetization flux ($\lambda_{m,T}$). Given that $L_{m,T}$ is bounded during normal and saturation conditions, as well as during GMDs—i.e., $L_{m,T}^{min} \leq L_{m,T} \leq L_{m,T}^{max}$, where $L_{m,T}^{min}$ and $L_{m,T}^{max}$ can be obtained from the magnetization curve of the transformer— element $\theta_T(.)$ varies between $\theta_T^{min}$ and $\theta_T^{max}$. As a result, matrix $A_T$ also varies between $A_T^{min}$ (when $L_{m,T} = L_{m,T}^{min}$) and $A_T^{max}$ (when $L_{m,T} = L_{m,T}^{max}$). Therefore, a linear combination of $A_T^{max}$ and $A_T^{min}$ via the coefficients $\mu_{T,1}$ and $\mu_{T,2}$ can be used to represent $A_T$, as shown below:

$$A_T = \mu_{T,1} A_T^{max} + \mu_{T,2} A_T^{min} \tag{4.16}$$

where:

$$\mu_{T,1} = \frac{\theta_T(\lambda_{m,T}) - \theta_T^{min}}{\theta_T^{max} - \theta_T^{min}} \tag{4.17}$$

$$\mu_{T,2} = 1 - \mu_{T,1} \tag{4.18}$$

combining (4.16) and (4.14) leads to the following polytopic form of transformers' state-space model:

$$\begin{cases} \dot{x}_T(t) = \sum_{i=1}^{2} \mu_{T,i} A_{T,i} x_T(t) + B_T u_T(t) \\ y_T(t) = C_T x_T(t) \end{cases} \tag{4.19}$$

where $A_{T,1} = A_T^{max}$ and $A_{T,2} = A_T^{min}$ are constant matrices, and coefficients $\mu_{T,1}$ and $\mu_{T,2}$ are time-varying parameters.

## 4.3 State Space Model of CTs

The equivalent circuit of CTs is shown in Fig. 4.2. In this figure, all the parameters are transferred to the primary side. The subscript $CT$ denotes the parameters of the CT, and $R_b$ and $L_b$ are the resistance and inductance of the burden connected to the CT. The rest of the parameters are similar to the ones explained in the previous section for transformers.

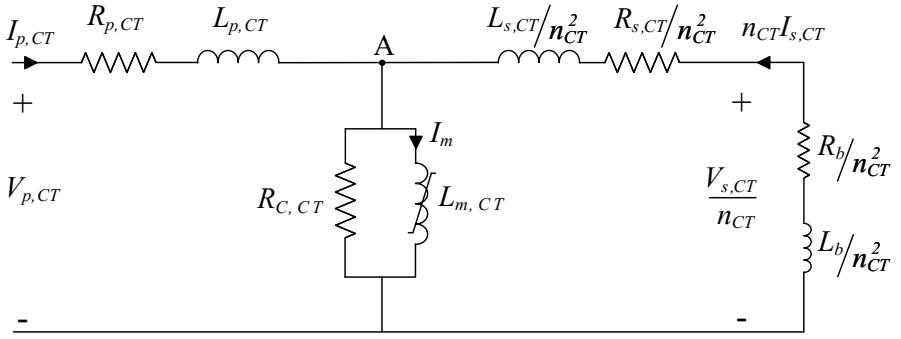


FIGURE 4.2: Equivalent circuit of CTs.

Given that the equivalent circuits of CTs and transformers are similar, (4.8)-(4.13) hold for CTs as well. However, since the secondary terminal of the CT is connected to a burden, $V_{s,CT}$ is not an input anymore and it can be calculated using the following equation:

$$V_{s,CT} = -R_b I_{s,CT} - L_b \frac{dI_{s,CT}}{dt} \tag{4.20}$$

Plugging the above equation into (4.12) and utilizing (4.9) results in

$$\frac{d\lambda_{2,CT}}{dt} = -\frac{R_b + R_{s,CT}}{L_b + L_{s,CT}}\lambda_{2,CT} + \frac{R_{s,CT} + R_b}{L_b + L_{s,CT}}\lambda_{m,CT} +$$

$$\frac{L_b}{L_b + L_{s,CT}}\frac{d\lambda_{m,CT}}{dt} \tag{4.21}$$

Substituting $\frac{d\lambda_{m,CT}}{dt}$ from (4.13) in (4.21) results in (4.22), which is shown at the top of the next page.

$$\begin{aligned}\frac{d\lambda_{2,CT}}{dt} = &\underbrace{\frac{R_{c,CT}L_b}{L_{p,CT}\left(L_b+L_{s,CT}\right)}}_{A_{21,CT}}\lambda_{1,CT}+\\ &\underbrace{\frac{\frac{n_{CT}^2 L_b R_{c,CT}}{L_{s,CT}}-R_b-R_{s,CT}}{L_b+L_{s,CT}}}_{A_{22,CT}}\lambda_{2,CT}+\\ &\underbrace{\frac{R_b+R_{s,CT}-\frac{L_b R_{c,CT}}{L_{p,CT}}-\frac{n_{CT}^2 L_b R_{c,CT}}{L_{s,CT}}-\frac{L_b R_{c,CT}}{L_{m,CT}(\lambda_{m,CT})}}{L_b+L_{s,CT}}}_{A_{23,CT}}\lambda_{m,CT}\end{aligned} \tag{4.22}$$

Using (4.11), (4.13), and (4.22), the state-space equations of CTs is obtained as follows:

$$\begin{cases}\dot{x}_{CT}(t) = A_{CT}x_{CT}(t) + B_{CT}V_{p,CT}(t)\\ I_{s,CT} = C_{CT}x_{CT}(t)\end{cases} \tag{4.23}$$

where

$$x_{CT} = \begin{bmatrix}\lambda_{1,CT} & \lambda_{2,CT} & \lambda_{m,CT}\end{bmatrix}^T \tag{4.24}$$

$$A_{CT} = \begin{bmatrix}-\frac{R_{p,CT}}{L_{p,CT}} & 0 & \frac{R_{p,CT}}{L_{p,CT}}\\ A_{21,CT} & A_{22,CT} & A_{23,CT}\\ \frac{R_{c,CT}}{L_{p,CT}} & \frac{n_{CT}^2 R_{c,CT}}{L_{s,CT}} & \theta_{CT}\left(\lambda_{m,CT}\right)\end{bmatrix} \tag{4.25}$$

$$B_{CT} = \begin{bmatrix}1 & 0 & 0\end{bmatrix}^T \tag{4.26}$$

$$C_{CT} = \begin{bmatrix}0 & \frac{n^2}{L_{s,CT}} & -\frac{n^2}{L_{s,CT}}\end{bmatrix} \tag{4.27}$$

and parameters $A_{21,CT}$, $A_{22,CT}$, and $A_{23,CT}$ are defined in (4.22). Additionally, $\theta_{CT}\left(\lambda_{m,CT}\right)$ is obtained from (4.15) by changing superscript $T$ to $CT$.

Similar to transformers, $L_{m,CT}$ of a CT is a function of its $\lambda_{m,CT}$, and is bounded between $L_{m,CT}^{min}$ and $L_{m,CT}^{max}$, both of which can be obtained from the magnetization curve of the CT. As a result, $\theta_{CT}(.)$ varies between $\theta_{CT}^{min}$ and $\theta_{CT}^{max}$, and thus matrix $A_{CT}$ also varies between $A_{CT}^{min}$ and $A_{CT}^{max}$. Therefore, a linear combination of these two matrices can be used to represent $A_{CT}$ at any time, as shown below:

$$A_{CT} = \mu_{CT,1}A_{CT}^{max} + \mu_{CT,2}A_{CT}^{min} \tag{4.28}$$

where:

$$\mu_{CT,1} = \frac{\theta_{CT}(\lambda_{m,CT}) - \theta_{CT}^{min}}{\theta_{CT}^{max} - \theta_{CT}^{min}} \tag{4.29}$$

$$\mu_{CT,2} = 1 - \mu_{CT,1} \tag{4.30}$$

Using (4.28), the state-space model of equation (4.23) can be presented in the following polytopic form:

$$\begin{cases} \dot{x}_T(t) = \sum_{i=1}^{2} \mu_i A_{T,i} x_T(t) + B_T u_T(t) \\ I_{s,CT}(t) = C_T x_T(t) \end{cases} \tag{4.31}$$

where $A_{CT,1} = A_{CT}^{max}$ and $A_{CT,2} = A_{CT}^{min}$ are constant matrices, and coefficients $\mu_{CT,1}$ and $\mu_{CT,2}$ are time-varying parameters.

## 4.4 Observer for LPV Systems

This section aims to synthesises observers for transformer and CT elements, enabling the provision of state estimation for those models. Observers are systems defined in state space, tailored to follow another system's states - typically called plant. Fig. 4.3 demonstrates connection between observer and a dynamic system (plant). Observers receive the input signal of plant and its output as a feedback, and seek to mimic plant's output. Plant is often a real world system, and it is reasonable to assume that plant's system is stable. However, observers are theoretically-designed systems and often are in the form of software, meaning that their stability must be ensured to successfully fulfil the purpose of state tracking. Next section explores the stability criteria in this regard.

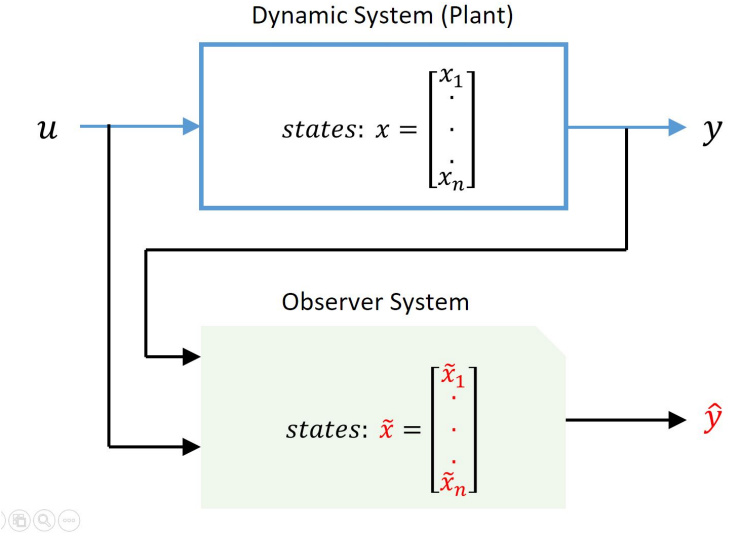


FIGURE 4.3: Observer and dynamic system connection for state estimation

### 4.4.1 Stability in LPV State Space Models

This section reviews the stability analysis for state space systems and LPV systems. Developed models for transformer and CT are stable since they are directly resulted from physical equation. Below methods give readers further knowledge on LPV systems stability. Observer design at at Sec. 4.4.3 is accompanied with stability checks in the observer design procedure. Additionally, one can verify stability of the transformer and CT models numerically with the below method.

Stability of Linear Time-Invariant (LTI) systems with constant coefficients can be examined by considering their natural response (response to zero input, $u(t) = 0$). Consider the LTI system below:

$$\begin{cases} \dot{x}(t) = Ax(t) + Bu(t) \\ y(t) = Cx(t) \end{cases} \tag{4.32}$$

These type of systems are said to be asymptotically stable if for any initial condition $x(0)$, system's states - i.e. vector $x$ - converges to zero vector (the origin for its space) as $t \to \infty$. In case the states don't converge to zero but remain in a boundary $\delta$ (i.e. $||x(t)|| < \delta$ as $t \to \infty$), then the system is said to be marginally stable [68].

Above definitions apply for the linear systems. However, the models presented for the transformer and CT in the previous sections are parameter varying. Due to the fact that those LPV systems have part of their parameters varying also with time, they are considered as non-linear systems, which require non-linear methods for examining their stability [69].

For non-linear systems, a common stability definition is Lyapunov's stability criterion. Considering the general non-linear systems of (4.1). First, the equilibrium point $x_e$ is defined as the point where system states don't move from that point unless input is applied, i.e. $f(x_e, 0) = 0$. Then, stability for a given system is stated such that: if the initial states are inside a certain boundary $\delta > 0$ of equilibrium point or $||x(0) - x_e|| < \delta$, then the states remain in any small arbitrary boundary $\epsilon$ of $x_e$ since a certain time $t \geq 0$ : $\|x(t) - x_e\| \leq \epsilon$ for $\forall \epsilon > 0$ [70].

A method known as Lyapunov's direct method provides a mathematical technique for validating the stability of systems as the following: Assume origin (zero vector) is an equilibrium point for the system $\dot{x}(t) = f(x(t))$ , i.e. it satisfies $f(0) = 0$. Assuming that there exists a differentiable function $V(x)$ with $V : D_x \to \mathbb{R}$, if the following conditions are met, then the system is asymptotically stable [70]:

- $V(x) > 0$ for $x \in D_x - \{0\}$
- $\dot{V}(x) \leq 0$ for $x \in D_x$

Although the Lyapunov's stability criterion is defined for non-linear systems, the extension of it for the specific case of LTI systems (which are a subset of non-linear systems) along with Lyapunov's direct stability method eventually gives a condition for stability of LTI systems in a compact form:

$$A^T P + PA = -Q \tag{4.33}$$

Where $Q$ is a chosen positive definite matrix. If the above equation has a solution for $P$ that is positive definite, then the system is said to be stable [70].

Now, stability for LPV systems is examined. Bearing in mind that LPV systems are a specific form of the general non-linear system defined above, they need to treated with non-linear stability techniques. Nevertheless, there exists a more relaxed condition for stability of LPV system known as Quadratic Stability (QS) based on the Lyapunov's stability, which can guarantee the stability for LPV systems over all of the parameter it can have for the system [71].

Assume an LPV system with varying parameters $\theta$ and the space $H$ as the space that all of values for the parameters $\theta$ span as below:

$$\dot{x}(t) = A(\theta)x(t) \tag{4.34}$$

This LPV system is stable if and only if a positive definite matrix $P$ exists such that for all the parameters $\theta \in H$:

$$A^T(\theta)P + PA(\theta) < 0 \tag{4.35}$$

Above definition is parameter varying but it's not time varying. For parameters that vary also over time, consider the following LPV system:

$$\dot{x}(t) = A(\theta(t))x(t) \tag{4.36}$$

This system is said to be quadratically stable if there exists a positive definite matrix $P$ for all of the matrices $\tilde{A}(.) = \{A(\theta) \quad | \quad \theta \in H\}$

$$\tilde{A}^T P + P\tilde{A} < 0 \tag{4.37}$$

Which in case of the polytopic form, the $\tilde{A}(.)$ turns into the set of the matrices with parameters in the vertices. Thus, LPV systems are stable when a common matrix $P$ is found [72, 73].

Additionally, it can be seen that above criterion is inherently related to the method of Lyapunov's stability in equation (4.33).

### 4.4.2 Observability

Observers estimate the states of the plant. For that to be feasible, the plant must be observable, i.e. all of its internal state can be determined via having the knowledge of input signal $u(t)$, and feedback signal (output, $y(t)$). Conversely, if a system is not observable, some of the internal states cannot be estimated merely by knowing the input and output given to that system. Observability of a system has applications in state estimation, filtering, and control of systems and is related to how the states are linked to the output [64].

There are criterion that can determine observability of systems. Regarding that LPV systems are time-varying systems, first a very general criterion for the observability of time-varying systems is introduced. Consider the time-varying system of (4.2). Assume $t_0$ is the initial moment and $x(t_0)$ is the initial condition. The solution for finding the state vector $x$ at time $t$ is given by:

$$x(t) = \Phi(t, t_0)x(t_0) + \int_{t_0}^{t} \Phi(t, \tau)B(\tau)u(\tau)\partial\tau \tag{4.38}$$

Where $\Phi(t, t_0)$ is the transition matrix defined as:

$$\Phi(t, t_0) = U(t)U^{-1}(t_0) \tag{4.39}$$

in which $U(t)$ is the called the fundamental solution matrix with $U(t_0) = I_n$ and $\dot{U}(t) = A(t)U(t)$.

Matrix $H(t, t_0)$ is defined as:

$$H(t, t_0) = \int_{t_0}^{t} \bar{\Phi}^T(\tau, t_0)\bar{C}^T(\tau)C(\tau)\Phi(\tau, t_0)\partial\tau \tag{4.40}$$

Then, if the matrix $H(t, t_0)$, calculated at time $t$, is positive definite, the system is said to be observable at time $t$ [64].

A simpler subset of time-varying systems are linear time-invariant (LTI) systems. Above criterion can be simplified for those type of systems. Consider LTI systems defined at

(4.32). Matrix $Q$ is formed as:

$$Q = \begin{bmatrix} C^T & A^T C^T & A^{2^T} C^T & \dots & A^{n-1^T} C^T \end{bmatrix} \tag{4.41}$$

Where $n$ is the number of states. If rank of matrix $Q$ is equal to the $n$, then the system is said to be observable [65].

Having introduced the above observability criteria, observability for LPV systems is given here. Consider the LPV systems with Polytopic form of (4.7). If all the individual pairs of $[A_i, C]$ are observable (in the sense of LTI system), then the above LPV system is said to be observable [67, 74].

### 4.4.3 LPV Observer Design

As shown in previous sections, transformers and CTs can be modeled by sets of LPV equations written in the polytopic form, i.e., (4.19) and (4.31), so requiring a specific type of observers to estimate their states. As shown in [66], such observers for transformers and CTs can be developed in the following structure

$$\begin{cases} \dot{z}(t) = \sum_{i=1}^{2} \mu_i N_i z(t) + Gu(t) + LY(t) \\ \tilde{x}(t) = z(t) + HY(t) \end{cases} \tag{4.42}$$

where $u(t)$ and $Y(t)$ are respectively the input and output of the system, e.g., $u_T(t)$ and $y_T(t)$ for transformers and $u_{CT}(t)$ and $y_{CT}(t)$ for CT, and $\tilde{x}(t)$ denotes the estimated states. Additionally, $N_i$, $L$, $G$, and $H$ are observer gains to be designed to make the observer accurate and stable.

To make the observer accurate, its error, which is defined as $e(t) = x(t) - \tilde{x}(t)$, must approach zero as $t \to \infty$. To fulfill this condition, the differential of the error, i.e., $\dot{e}(t) = \dot{x}(t) - \dot{\tilde{x}}(t)$, should be asymptotically stable. By using (4.42) and (4.19) or (4.31), $\dot{e}(t)$ is obtained as follows:

$$\begin{aligned} \dot{e}(t) = \sum_{i=1}^{2} \mu_i \{ [(I - HC)A_i + N_i HC - LC]x(t) - N_i \tilde{x}(t) \} \\ + [(I - HC)B - G]\, u(t) \end{aligned} \tag{4.43}$$

By defining $M = I - HC$, $\dot{e}(t)$ is reduced to (4.44) if (4.45) and (4.46) are met:

$$\dot{e}(t) = \sum_{i=1}^{2} \mu_i N_i e(t) \tag{4.44}$$

$$MA_i - N_iM - LC = 0 \quad \forall i \in \{1, 2\} \tag{4.45}$$

$$MB - G = 0 \tag{4.46}$$

Therefore, as (4.44) shows, the error approaches zero if $\mu_1 N_1 + \mu_2 N_2$ is stable, i.e., all its eigenvalues are in the left half plane. As shown in [66] and stated previously in 4.4.1, this condition is met if there exists a common positive definite symmetric matrix $P$ such that:

$$N_i^T P + P N_i < 0 \quad \forall i \in \{1, 2\} \tag{4.47}$$

Therefore, satisfying (4.45)-(4.47) guarantees that the observer's error approaches asymptotically to zero, and thus the states of the transformer and its CTs can be accurately estimated. Design of observer thus entails finding observer gains $N_i$, $G$, $L$, and $H$ by plugging in the system's matrices - $A_i$, $B$, and $C$ - into (4.45)-(4.47) and satisfying them.

## 4.5 Transformer and CT Observers

Given above LPV models for transformer and CT, and the LPV observer design procedure, this section lucidly expresses the LPV observer equations for transformer and CT. These equations are the concrete equations used for the proposed framework introduced in the next chapter.Fig. 4.4 shows observer input and outputs related to the circuit of transformer and CT.

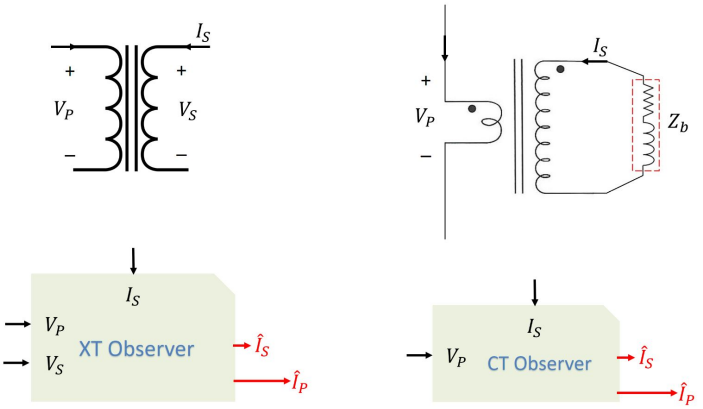


FIGURE 4.4: Observer inputs-outputs regarding the transformer (XT) and CT circuit

### 4.5.1 Transformer LPV Observer

Adopting the LPV observer of (4.42) for the transformer LPV model specified at (4.14) gives the following LPV observer system:

$$\begin{cases} \dot{z}(t) = \sum_{i=1}^{2} \mu_i N_i z(t) + G \begin{bmatrix} V_{p,T}(t) \\ V_{s,T}(t) \end{bmatrix} + L I_{s,T}(t) \\ \hat{x}_T(t) = z(t) + H I_{s,T}(t) \end{cases} \tag{4.48}$$

where $\hat{x}_T(t)$ is the estimation of transformer states, i.e. estimated fluxes $\hat{x}_T = \begin{bmatrix} \hat{\lambda}_{1,T} & \hat{\lambda}_{2,T} & \hat{\lambda}_{m,T} \end{bmatrix}^T$.

### 4.5.2 CT LPV Observer

Adopting the LPV observer of (4.42) for the CT LPV model specified at (4.31) gives the following LPV observer system:

$$\begin{cases} \dot{z}(t) = \sum_{i=1}^{2} \mu_i N_i z(t) + G V_{p,CT}(t) + L I_{s,CT}(t) \\ \hat{x}_{CT}(t) = z(t) + H I_{s,CT}(t) \end{cases} \tag{4.49}$$

where $\hat{x}_{CT}(t)$ is the estimation of CT states, i.e. estimated fluxes $\hat{x}_{CT} = \begin{bmatrix} \hat{\lambda}_{1,CT} & \hat{\lambda}_{2,CT} & \hat{\lambda}_{m,CT} \end{bmatrix}^T$.

# Chapter 5

# Detecting Internal Faults During GMDs

The proposed solution to address the problem described in Chapter 3 includes two main schemes (Fig. 5.1). The first scheme addresses the saturation problem of CTs during GMDs by estimating the primary current of CTs based on their secondary current. Thus, after implementing this scheme, the 87T element makes protective decisions based on estimated primary currents, instead of the distorted secondary currents of their CTs. The second scheme, on the other hand, detects internal faults during GMDs.

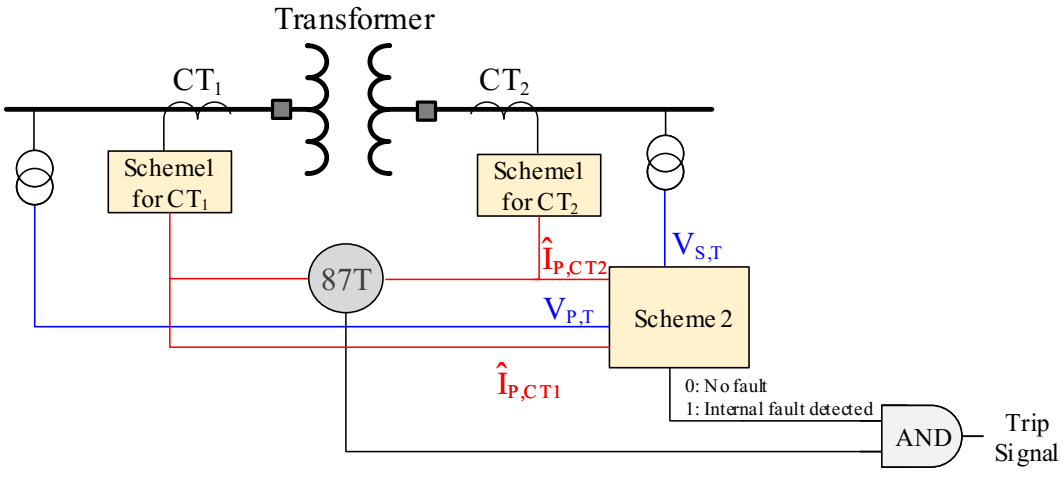


FIGURE 5.1: Proposed CT correction and internal fault detection in the presence of GMDs.

The observers defined and designed in the previous chapter are embedded in these two schemes. Scheme 1 is internally an LPV CT observer, and scheme 2 makes use of the transformer LPV observer. The following sections elaborate on these two schemes in detail.

## 5.1 Scheme 1: CT Correction During GMDs

As shown in Chapter 3, the DC component added to the current of CTs during GMDs can saturate the core of CTs, thus distorting their secondary currents. Such distortion might result in malfunction of the 87T element, or paralyze its operation. Scheme 1 in this study is developed to eliminate the impacts of saturation from measurements by accurately estimating the primary currents of CTs using their secondary currents, primary voltages, and state state models.

To this aim, first the polytopic form of each CT's state space model is developed according to (4.31) in section 4.3. To estimate the primary current of a CT, the observer introduced in Section 4.5.2 is used. At each time-step, this observer uses the secondary current of the CT (i.e., $I_{s,CT}$) and its primary voltage (i.e., $V_{p,CT}$) to update the estimation of the CT states, i.e. $\hat{x}_{CT}$. Measurement of secondary current of CT is naturally available. Since CTs are connected in series and have only one turn in their primary side, the voltage across the primary winding is low, which allows for direct measurement without needing a voltage transformer. Additionally, given that the core of each CT is modeled by a time-variant magnetizing inductor (i.e., $L_{m,CT}$) and a parallel resistor, the value of the magnetizing inductor, and accordingly coefficients $\mu_{CT,1}$ and $\mu_{CT,2}$, at any time-step are calculable via (4.29), (4.30), and $L = \frac{\lambda}{I}$. $L_{m,CT}$ can be calculated using the CT's magnetization characteristic curve (flux-current) based on the estimated core flux (i.e., $\lambda_{m,CT}$) in the previous time-step, and $\mu_{CT,1}$ and $\mu_{CT,2}$ are computed from that. As explained in Chapter 4, magnetization characteristic of CTs are often provided by manufacturers or can be obtained by an excitation test [67]. Once the states of the CT are estimated for a time-step, its primary current ($I_{p,CT}$) is calculated using (4.8). Thus, during GMDs, the relay can use the estimated primary currents of its CTs obtained from Scheme 1, instead of their distorted secondary currents.

## 5.2 Scheme 2: Internal Fault Detection in the Presence of GMDs

To detect internal faults during GMDs, this study develops Scheme 2, which estimates the primary current of the transformer (i.e., $\hat{I}_{p,T}$) via an observer unit, and compares it with the measured one (i.e., $I_{p,T}$) by means of a residual function unit.

In a transformer, when there is no internal fault and the transformer is functioning normally, the model based on which Scheme 2 operates (i.e., equation (4.19)) perfectly matches and represents the actual transformer, thus no discrepancy must occur between

the measured and estimated primary currents. Nonetheless, in cases of internal faults, the estimated primary current deviates from the actual value since the state space model previously constructed fails to accurately represent the transformer (and the observer is designed based on the model). On this basis, the observer introduced in Section 4.5.1 is used to estimate the states of the transformer to compare the $I_{p,T}$ with its estimation. The observer estimation for transformer is based on (4.19), and by using the primary and secondary voltages of the transformer (i.e., $V_{p,T}$ and $V_{s,T}$). Given that the magnetizing inductor of the transformer (i.e., $L_{m,T}$) is time-variant—since its value at any time-step depends on the core's flux ($\lambda_{m,T}$)—-it is calculated at every time-step based on the estimated flux at the previous time-step and the transformer's excitation curve (flux - current curve). Using the obtained magnetization inductor, $L_{m,T}$, the observer calculates coefficients $\mu_{1,T}$ and $\mu_{2,T}$ based on (4.17) and (4.18). Once the states of the transformer are estimated for a time-step, its primary current at that time-step can be calculated using (4.8).

Having the measurement and estimation of transformer primary current, internal faults during GMDs can be detected by monitoring a Residual Function (RF) defined in (5.1), and comparing it against a threshold ($\delta$); that is, an internal fault has happened if

$$\underbrace{\left|\frac{I_{p,T}(t) - \hat{I}_{p,T}(t)}{I_{p,T(t)}}\right|}_{RF(t)} \geq \delta \tag{5.1}$$

If (5.1) is met, the output of Scheme 2—which is ANDed with the output of the 87T element—becomes one. Thus the transformer is tripped only if both 87T element and Scheme 2 pick up.

Putting the proposed framework into practice entails implementation of Scheme 1 and Scheme 2 inside the 87T's software which involves two CT observer units and one transformer unit along with residual function. These units require observer gains which are obtained through the observer design defined at section. 4.4.3. This is a one-time procedure design that must be done for CT1, CT2, and the transformer after their parameters are obtained - either via tests or available commercial data-sheets. Afterwards, threshold $\delta$ can be fine-tuned practically for the healthy transformer while it is operating. Further more, threshold can be set higher in order to provide safety margin for practical purposes. This threshold accounts for parameter variations, noise, and other sources of error. Software of Scheme 1 and Scheme 2 should be created such that it is ensured that their processing time is less than a time step.

# Chapter 6

# Performance Evaluation

To evaluate the proposed technique, the 118-bus test system introduced in Chapter 2 is utilized, and two GMD phenomena are simulated in EMTP-RV software with different severities, that is, the magnitude of reference $GEF$ is assumed to be 4 V/km and 10 V/km. The proposed technique is simulated in MATLAB for T46 and its associated CTs, and its performance is corroborated under various operating conditions. Without loss of generality, this chapter present the results for Phase-A of CT1 and T46. Same results can be achieved for CT2 and other phases a well.

## 6.1 CT Correction During GMDs

This section probes into the performance of Scheme 1, introduced in Section 6.1, under normal conditions, during GMDs, and when the transformer is experiencing a fault in the presence of GICs. For all these scenarios, the estimated primary current ($\hat{I}_{p,CT1}$), actual primary current ($I_{p,CT1}$), and actual secondary current transferred to the primary ($n_{CT1}\hat{I}_{s,CT1}$) are obtained and compared.

**• Scenario 1: Normal operation and at the beginning of GMDs**

In this scenario, the transformer is operating under normal condition before a GMD starts at $t = 0.5$ s. Fig. 6.1 demonstrates the performance of Scheme 1 under two GMDs with severities of 4 V/km and 10 V/km. As this figure shows, in both cases, an exponential DC component shifts the CT primary current up immediately after GMDs start. The DC component is larger when the GMD is more severe. In both cases, the estimated primary current of CT1 perfectly overlaps the actual primary current before and during GMDs, indicating that Scheme 1 is capable of estimating the primary

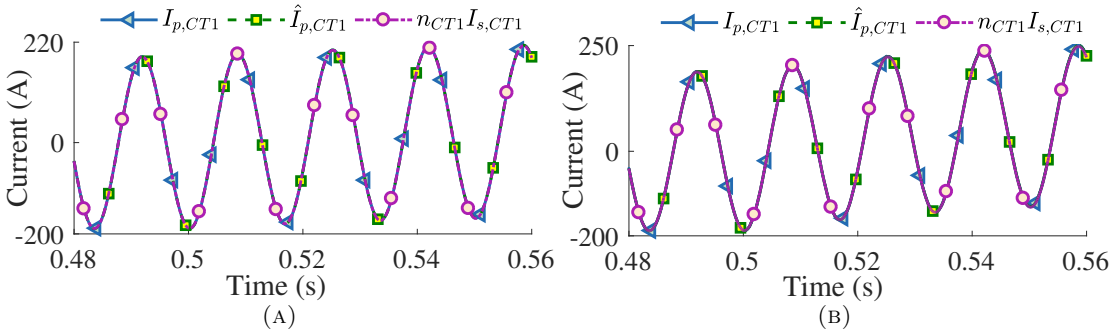


FIGURE 6.1: Estimated and actual currents of CT1 during Scenario 1: A) $GEF = 4$ V/km, and B) $GEF = 10$ V/km.

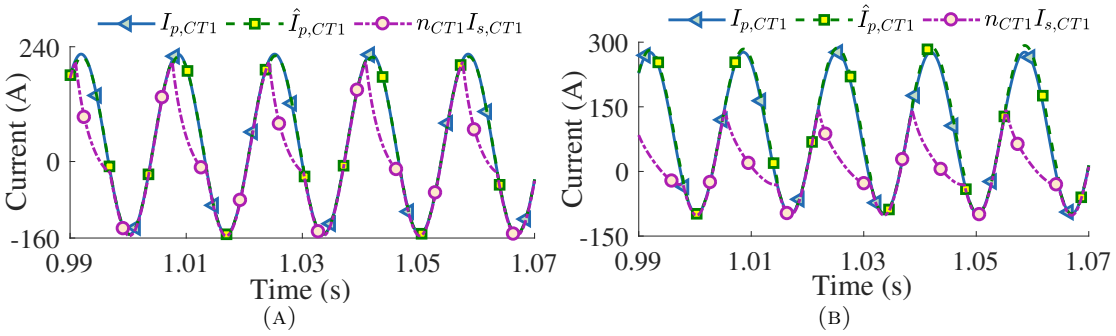


FIGURE 6.2: Estimated and actual currents of CT1 during Scenario 2: A) $GEF = 4$ V/km, and B) $GEF = 10$ V/km.

current of CTs in the absence and presence of GICs. The reason for such an accurate performance is that the state-space model developed for CTs correctly presents them during GMDs, so the primary current is accurately estimated.

- **Scenario 2: CT saturation due to GICs**

Immediate rise of the DC component caused by the GMD is later on followed by another slow rise pertaining to the transformer (T46), as previously explained in chapter 3. This high-magnitude DC component effectively pushes CT1 into its saturation region. the severity of saturation depends upon the magnitude of the DC component, which pertains to the severity of the GMD. Fig. 6.2 shows the actual primary and secondary current waveforms, as well as the estimated primary current, from $t = 0.99$ s, i.e., when the CT is severely saturated in both GMD cases. As Fig. 6.2 shows, the estimated current closely follows the actual one, while the CT's secondary current is distorted due to saturation. Thus this scenario clearly indicates that the proposed scheme accurately estimates the primary current of CTs, regardless of the severity of the GMD phenomenon.

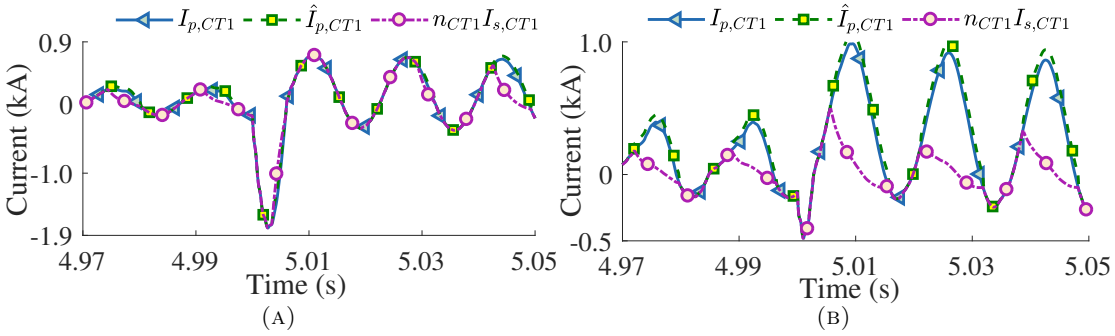


FIGURE 6.3: Estimated and actual currents of CT1 during Scenario 3: A) $GEF = 4$ V/km, and B) $GEF = 10$ V/km.

- **Scenario 3: Internal faults during GMDs**

Similar to the previous two scenarios, the GMDs of this scenario start at $t = 0.5$ s. Later on at $t = 5$ s, i.e., when the CT is saturated due to GICs, a 15% TT fault happens at the secondary winding of T46. As a result of this fault, a large current flows in to the transformer and CT1 saturates more severely. Figs. 6.3-(a) and (b) illustrate the current waveforms of CT1 when the magnitude of reference $GEF$ is 4 V/km and 10 V/km, respectively. As this figure shows, $\hat{I}_{p,CT}$ remains accurate while the CT is experiencing a high-magnitude current during the fault, proving the ineffectiveness of transformer internal faults on the accuracy of Scheme 1.

## 6.2 Internal Fault Detection During GMDs

This section evaluates the performance of Scheme 2 for T46 under various conditions, i.e., during normal operation, when the transformer is saturated due to GICs, and under internal faults. Additionally, it investigates the impacts of system loading condition on the performance of the proposed technique. For each scenario, the estimated and actual primary currents of the transformer are compared, and the associated RF is obtained. As explained in Chapter 5, the RF must ideally remain at zero when no internal fault has happened. However, even a small internal fault increases the RF and deviates the estimated primary current from the actual one. This deviation is used to detect internal faults.

- **Scenario 4: Normal operation and at the beginning of GMDs**

Similar to previous scenarios, two GMD cases with reference GEFs of 4 V/km and 10 V/km start at $t = 0.5$ s. In both cases, Scheme 2 estimates the primary current of

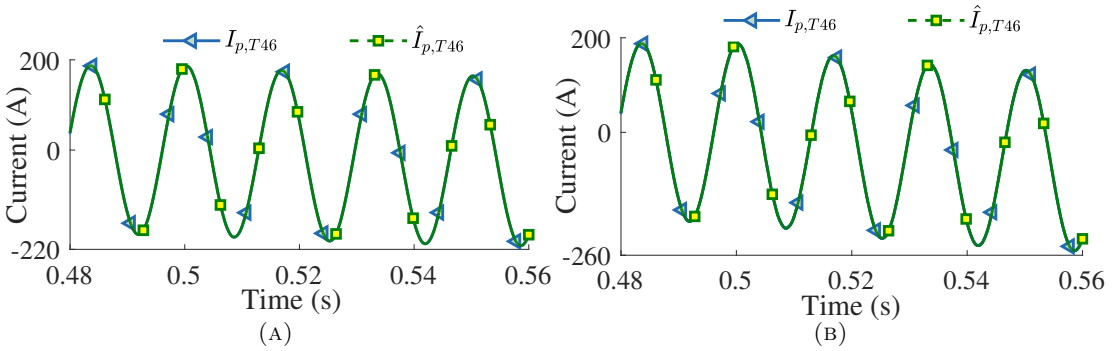


FIGURE 6.4: Estimated and actual primary currents of T46 during Scenario 4: A) $GEF = 4$ V/km, and B) $GEF = 10$ V/km.

the transformer using the procedure explained in Section 5.2. Fig. 6.4 shows the actual ($I_{p,T46}$) and estimated primary ($\hat{I}_{p,T46}$) currents of T46 before and after the GMD starts. As seen in the figure, Scheme 2 continues to accurately estimate the primary current regardless of the GEF magnitude and the DC exponential component. The reason for this accuracy is that the model based on which Scheme 2 operates does not change when GMDs start, and this model perfectly represent the transformer. Thus, estimation of the primary current remains accurate, and $RF(t)$, which is calculated based on (5.1), does not grow. As a result, Scheme 2 does not pick up, and its output remains zero.

- **Scenario 5: Transformer saturation due to GICs**

The previous scenario showed that the accuracy of Scheme 2 is maintained after the initiation of GMDs. This scenario proves that this scheme will remain accurate during the whole GMD phenomenon, even when the transformer saturates severely. Following the initiation of GMDs at $t = 0.5$ s and the initial rise of the DC component, T46 begins to slowly saturate, as discussed in chapter 3. After a while, e.g., at $t = 4$ s, the transformer is saturated, and thus its secondary current is highly distorted. Fig. 6.5 illustrates the actual and estimated primary currents of T46 when the transformer is saturated during both GMD cases. As this figure shows, although the transformer's secondary current ($I_{s,T46}$) is distorted, the estimated signal perfectly overlaps the primary current in both cases. As explained in the previous scenario, the reason for such accuracy is that the model based on which the observer operates remains accurate during saturation, and as a result the primary current is estimated accurately. As a result, this scenario corroborates the effectiveness of Scheme 2 when transformers are saturated due to GICs.

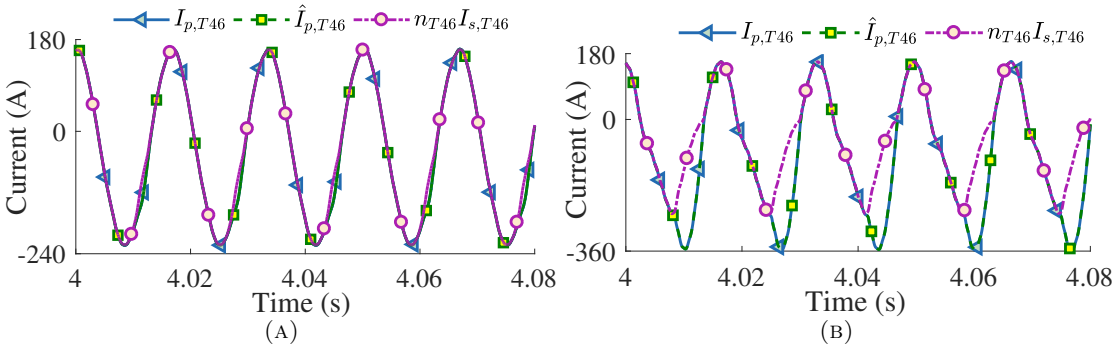


FIGURE 6.5: Estimated and actual primary currents of T46 during Scenario 5: A) $GEF = 4$ V/km, and B) $GEF = 10$ V/km.

**• Scenario 6: Internal faults during GMDs**

To evaluate the performance of Scheme 2 under internal faults, four fault cases are simulated at the secondary winding of T46: (i) a 15% TT fault, (ii) a 75% TT fault, (iii) a 15% Turn-to-Ground (TG) fault, and (iv) a 75% TG fault. All faults happen at $t = 5$ s, in the presence of GMDs that have already started since $t = 0.5$ s and their reference GEFs are 4 V/km and 10 V/km. Figs. 6.6-6.13 illustrate the actual and estimated primary currents of T46 and associated RFs during the above-mentioned fault cases. As sub-figure (a) of all figures show, the transformer current increases in all cases as soon as the faults happen. Given that the faults alter the transformer model, the estimated values deviate from the actual ones immediately after the faults start (sub-figure (a) of Figs. 6.6-6.13). This is due to the fact that the observer is designed based on the model of the healthy transformer, but the actual transformer is faulty. Therefore, as Sub-figure (b) of Figs. 6.6-6.13 show, the RF of the observer—which was nearly zero before the faults happen—suddenly increases significantly upon initiation of the faults, signifying that an internal fault is in progress. As Figs. 6.6-6.13 show, the extent of growth in the RF depends on 1) the type of the fault (TT vs. TG), 2) the intensity of the fault (15% vs. 75%), and 3) the severity of the GMD (4 V/km vs. 10 V/km). As this scenario proved, Scheme 2 accurately detects internal faults in the presence of GICs immediately after their occurrence, and its performance is not affected by the severity of GMDs.

**• Scenario 7: Impacts of transformer's loading condition on the proposed schemes**

To investigate the impacts of transformer loading condition on the proposed schemes, the load of T46—which was 30.24 MVA (nominal load) with 0.94 lagging power factor in previous scenarios—is changed in this scenario. To this aim, this scenario considers two cases: (i) the transformer is underloaded and delivers 80% of its nominal load at

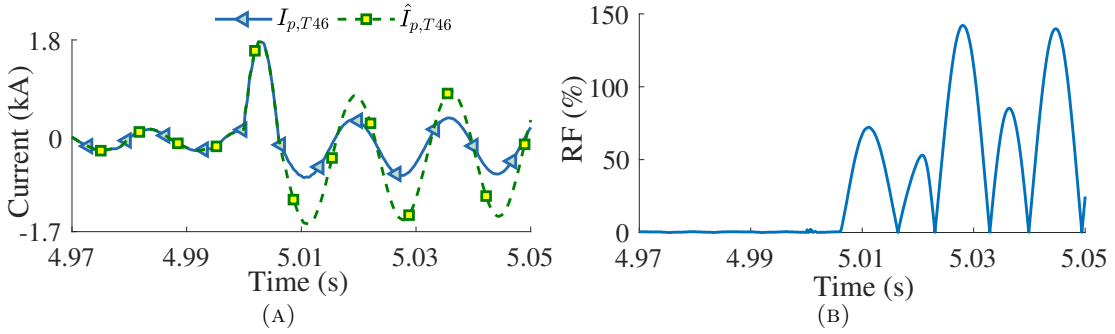


(A) (B)

FIGURE 6.6: (A) Actual and estimated primary currents, and (B) RF for a 15% TT fault during a GMD with reference GEF of 4 V/km.

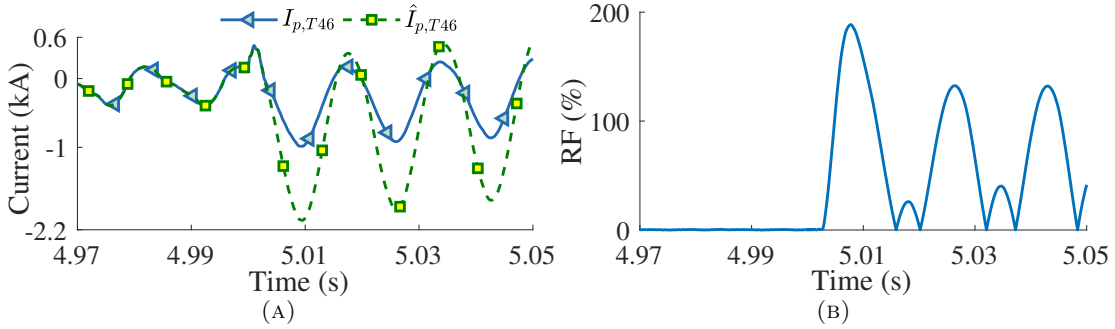


(A) (B)

FIGURE 6.7: (A) Actual and estimated primary currents, and (B) RF for a 15% TT fault during a GMD with reference GEF of 10 V/km.

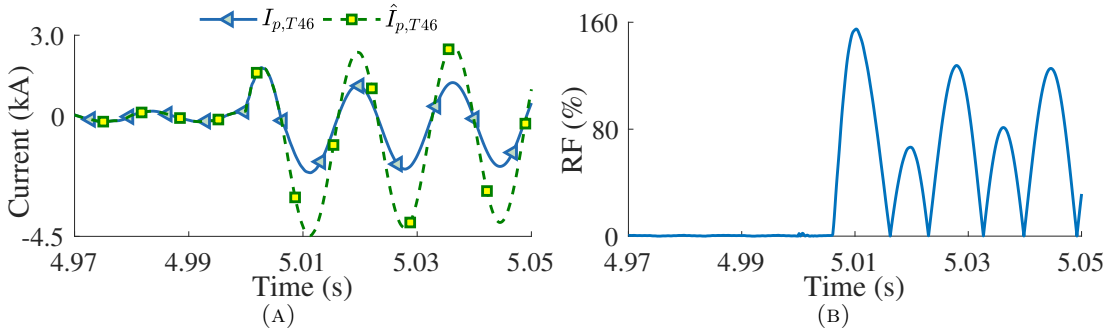


(A) (B)

FIGURE 6.8: (A) Actual and estimated primary currents, and (B) RF for a 75% TT fault during a GMD with reference GEF of 4 V/km.

0.7 lagging power factor during a GMD with reference GEF of 4 V/km, and (ii) the transformer is overloaded and delivers 120% of its nominal load at 0.9 leading power factor during a GMD with reference GEF of 10 V/km. In both cases, the GMD has started at $t = 0.5$ s, and a 15% TT fault happens at $t = 5$ s, when T46 and its CTs are severely saturated due to GICs. Figs. 6.14 and 6.15 show the estimated and actual primary currents of T46 and associated RF for cases (i) and (ii). As these figures show, in both cases the observer accurately estimates the primary current (i.e., the RFs are about zero) before the internal fault happens. However, as soon as the fault starts, the estimated and actual primary currents do not overlap anymore and the RF

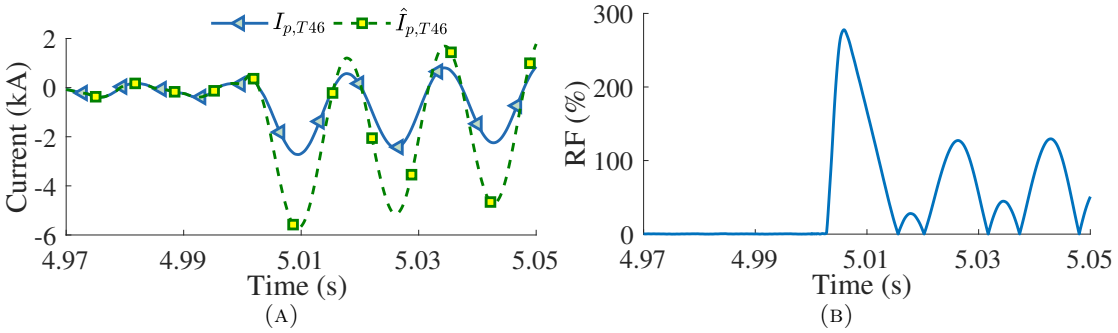


(A) (B)

FIGURE 6.9: (A) Actual and estimated primary currents, and (B) RF for a 75% TT fault during a GMD with reference GEF of 10 V/km.

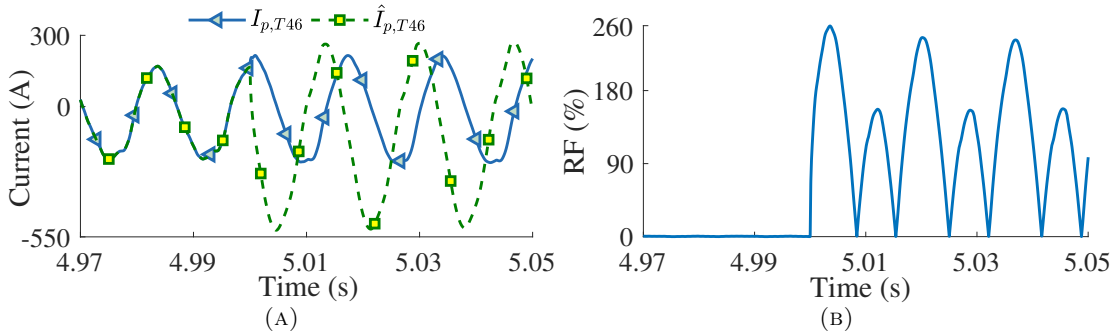


(A) (B)

FIGURE 6.10: (A) Actual and estimated primary currents, and (B) RF for a 15% TG fault during a GMD with reference GEF of 4 V/km.

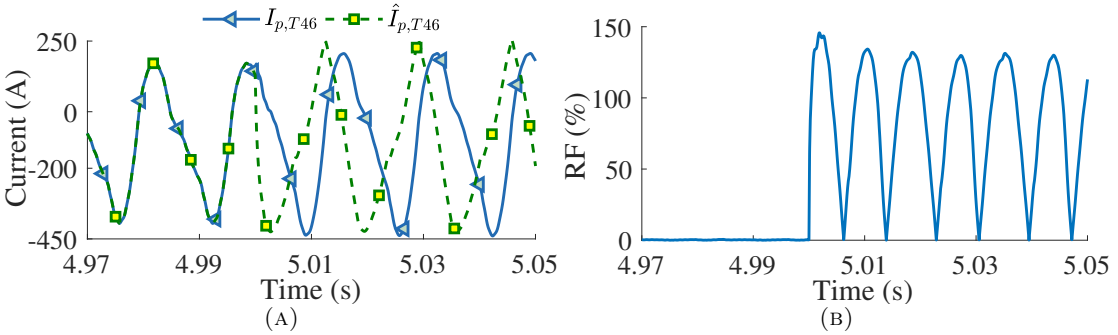


(A) (B)

FIGURE 6.11: (A) Actual and estimated primary currents, and (B) RF for a 15% TG fault during a GMD with reference GEF of 10 V/km.

increases, indicating that a fault is in progress. As a result, as this scenario illustrated, the performance of the proposed framework is not affected by loading condition of the transformer, since load variations do not change the transformer model.

This chapter evaluated the performance of Scheme 1 and Scheme 2. As simulations have shown, the presence of GICs causes CT and transformer saturation. The performance of Scheme 1 - which compensates for the distorted CT waveforms - is demonstrated for the following three scenarios: normal operation, the beginning of GMDs, saturated CTs, and internal faults of the transformer. Afterward, the performance of Scheme 2 is

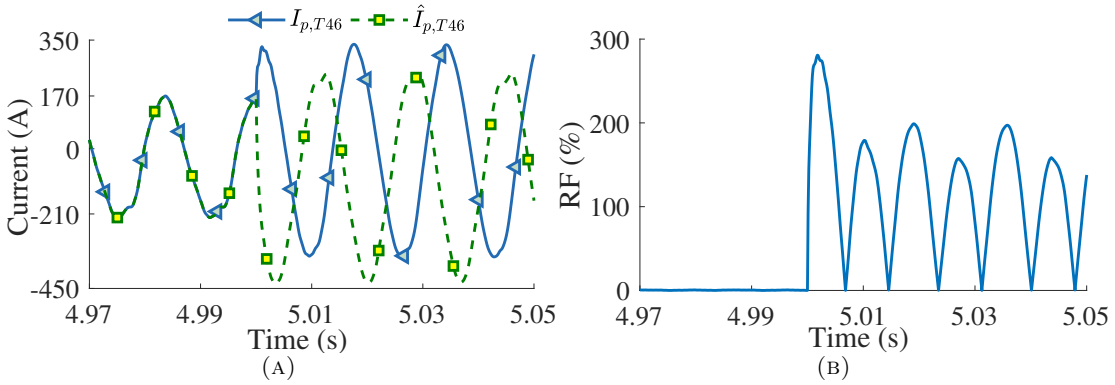


FIGURE 6.12: (A) Actual and estimated primary currents, and (B) RF for a 75% TG fault during a GMD with reference GEF of 4 V/km.

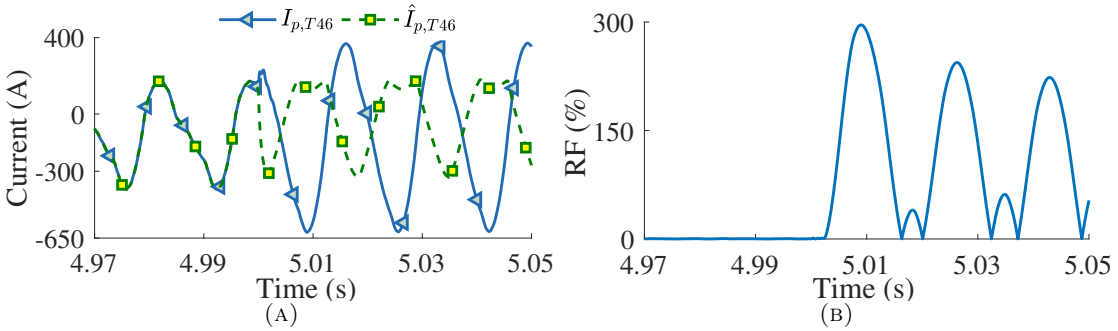


FIGURE 6.13: (A) Actual and estimated primary currents, and (B) RF for a 75% TG fault during a GMD with reference GEF of 10 V/km.

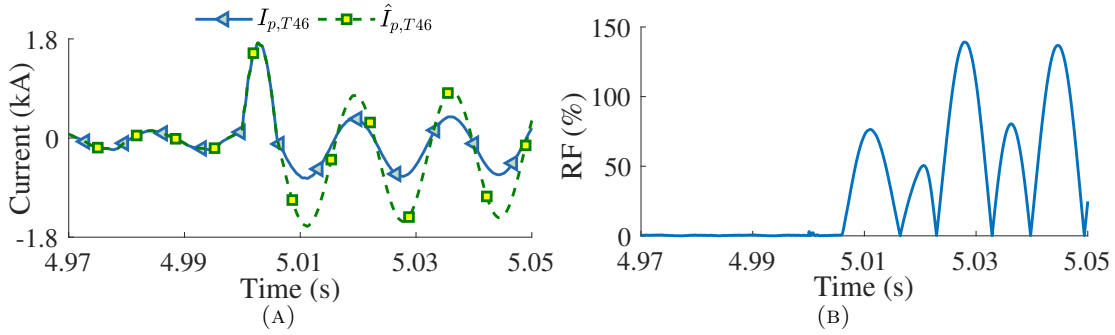


FIGURE 6.14: (A) Actual and estimated primary currents, and (B) RF for case (i) of Scenario 7.

demonstrated by means of four different scenarios in order to showcase its performance for internal fault detection. These four scenarios include 15% and 75% TT and TG internal faults occurring at the transformer. The effect of transformer's load condition on Scheme 2 is also examined for both under-load and over-load conditions. These seven scenarios illustrated that Scheme 1 and Scheme 2 can successfully be employed in 87T in order to accurately detect faults during GICs.

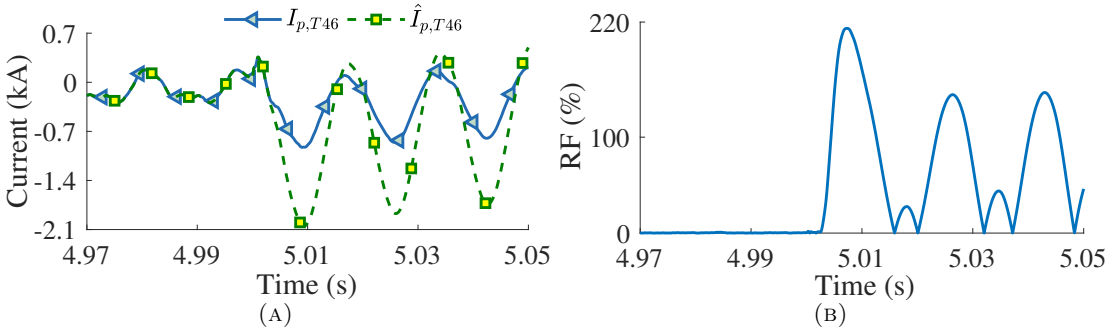


FIGURE 6.15: (A) Actual and estimated primary currents, and (B) RF for case (ii) of Scenario 7.

# Chapter 7

# Conclusion and Future WorK

## 7.1 Conclusion

This study first proved that off-the-shelf transformer differential relays may malfunction if an internal fault happens during a GMD. The reason is that the HB or HR elements of differential relays might block the tripping signal or add extra restraint, respectively, causing the fault to remain uninterrupted. To address this problem, this study proposed an auxiliary framework for single-phase transformers or three-phase transformer banks. This framework utilizes the LPV state-space equations of a power transformer and its CTs, and represents them in the polytopic form. The framework also employs LPV observers to estimate the state of the transformer and its CTs. To address the above-mentioned problem, the proposed framework benefits from two schemes: (i) CT correction and (ii) internal fault detection. The first scheme uses the estimated states of CTs to precisely calculate their primary currents. Thus, this scheme enables the differential relay to use the estimated primary currents of its CTs rather than their distorted secondary currents. The second scheme, on the other hand, uses the estimated states of a transformer to calculate its primary current. Then, this scheme detects internal faults of by comparing the estimated primary current of the transformer with the measured one, i.e., a large difference between the two signifies an internal fault. Simulation results obtained from EMTP-RV and MATLAB for various scenarios during two cases of GMD with low and high intensities corroborated the effectiveness of the proposed framework.

## 7.2 Future Work

1. GMD impacts on transformer differential protection has been reviewed in this study. As stated in section 1, GICs can impact other components such as generators. Harmonics introduced by GICs can cause damage to the rotor of generator. Static Var Compensators (SVCs) are also prone to these harmonics. In the future, methods can be devised for protection of generators, SVCs, and other equipment that may be harmed in the presence of GICs.

2. This study utilized two schemes containing LPV observers and residual functions to tackle the maloperation of 87T scheme in the presence of GICs. Machine learning techniques can be explored in the future to examine their behavior for addressing this problem, and to examine whether they can offer additional benefits to this problem.

3. This study assumes that the parameters of transformers and CTs do not change over time and design observers based on this assumption. In case that transformer parameters change over time or have measurement errors, ML approaches can be designed to minimize the error of the observer in such situations.

# Appendix A

# Publication

The author of this study has submitted the following publication during his master's studies:

[1] **M. Zandian**, A. Ameli, M. Ghafouri, R. Hassani, "A Framework to Avoid Maloperation of Transformer Differential Protection under Geomagnetic Disturbances", *IEEE Transactions on Power Delivery*, Mar., 2023

# Bibliography


[1] D.H. Boteler. Calculating the voltages induced in technological systems during a geomagnetic disturbance. 41(4):398–402, 1999. doi: 10.1109/15.809834.

[2] John G Kappenman. Geomagnetic storms and their impact on power systems. *IEEE Power Engineering Review*, 16(5), 1996.

[3] J. G. Kappenman, V. D. Albertson, and N. Mohan. Current transformer and relay performance in the presence of geomagnetically-induced currents. *IEEE Power Engineering Review*, PER-1(3):23–24, 1981. doi: 10.1109/MPER.1981.5511302.

[4] John T Gosling. The solar flare myth. *Journal of Geophysical Research: Space Physics*, 98(A11):18937–18949, 1993.

[5] DH Boteler. Space weather effects on power systems. *GEOPHYSICAL MONOGRAPH-AMERICAN GEOPHYSICAL UNION*, 125:347–352, 2001.

[6] Geomagnetic disturbance effects on power systems. *IEEE Transactions on Power Delivery*, 8(3):1206–1216, 1993. doi: 10.1109/61.252646.

[7] Layers of the sun. https://www.nasa.gov/mission_pages/iris/multimedia/layerzoo.html, . Accessed: 2023-03-29.

[8] Sunspots and solar flares. https://spaceplace.nasa.gov/solar-activity/en/, . Accessed: 2023-03-29.

[9] Corona. https://www.britannica.com/science/corona-Sun. Accessed: 2023-03-29.

[10] M.J. Aschwanden, S. Tilman, D. Breuer, and T.V. Johnson (Eds.). The sun. In *Encyclopedia of the solar system. (3rd ed.)*. 2014. URL https://search.credoreference.com/content/entry/estsolar/the_sun/1?institutionId=7307.

[11] John Cullerne. Sunspots. In *The Penguin Dictionary of Physics*. Penguin, 4th edition, 2009. URL https://search.credoreference.com/content/entry/pendphys/sunspots/0?institutionId=7307.

[12] Zhanle Du. Correlations between cme parameters and sunspot activity. *Solar Physics*, 278(1):203–215, 2012.

[13] H. Alfvén. On the theory of magnetic storms and aurorae. *Tellus*, 10(1):104–116, 1958. doi: 10.3402/tellusa.v10i1.9213. URL https://doi.org/10.3402/tellusa.v10i1.9213.

[14] Bogdan Kasztenny, Douglas Taylor, and N Fischer. Impact of geomagnetically induced currents on protection current transformers. In *Proceedings of the 13th International Conference on Developments in Power System Protection, Edinburgh, UK*, pages 7–10, 2016.

[15] Vipul N Rajput, David H Boteler, Nishil Rana, Mahenaj Saiyed, Smit Anjana, and Meet Shah. Insight into impact of geomagnetically induced currents on power systems: Overview, challenges and mitigation. *Electric Power Systems Research*, 192:106927, 2021.

[16] NASA. What is the solar cycle? https://spaceplace.nasa.gov/solar-cycles/en/. Accessed: 2023-03-31.

[17] NASA Astronomy. The next sunspot cycle. https://sten.astronomycafe.net/sunspot-cycle/. Accessed: 2023-03-31.

[18] Wikipedia. Solar cycle. https://en.wikipedia.org/wiki/Solar_cycle, . Accessed: 2023-03-31.

[19] SOLEN March 1 2023. Solar terrestrial activity report. https://en.wikipedia.org/wiki/Solar_cycle. Accessed: 2023-03-31.

[20] Holly Zell. Nasa - sun-earth connection. https://www.nasa.gov/mission_pages/themis/auroras/sun_earth_connect.html. Accessed: 2023-03-31.

[21] Sam Kneller. Atmosphere composed of five layers. https://theexplanation.com/earths-atmosphere-ingredients-life/atmosphere-composed-of-five-layers/. Accessed: 2023-03-31.

[22] Daisy Dobrijevic. Earth's magnetic field: Explained. https://www.space.com/earths-magnetic-field-explained. Accessed: 2023-03-31.

[23] Wikipedia. Ionosphere. https://en.wikipedia.org/wiki/Ionosphere, . Accessed: 2023-03-31.

[24] North American Electric Reliability Corporation. Effects of geomagnetic disturbances on the bulk power system, 2012.

[25] Risto Pirjola. Geomagnetically induced currents during magnetic storms. *IEEE transactions on plasma science*, 28(6):1867–1873, 2000.

[26] Navin Chandra Joshi, Neeraj Singh Bankoti, Seema Pande, Bimal Pande, and Kavita Pandey. Relationship between interplanetary field/plasma parameters with geomagnetic indices and their behavior during intense geomagnetic storms. *New Astronomy*, 16(6):366–385, 2011. ISSN 1384-1076. doi: https://doi.org/10.1016/j.newast.2011.01.004.

[27] C. A. Loewe and G. W. Prölss. Classification and mean behavior of magnetic storms. *Journal of Geophysical Research: Space Physics*, 102(A7):14209–14213, 1997.

[28] Barbara B Poppe. New scales help public, technicians understand space weather. *Eos, Transactions American Geophysical Union*, 81(29):322–328, 2000.

[29] D. H. Boteler and R. J. Pirjola. Modeling geomagnetically induced currents. *Space Weather*, 15(1):258–276.

[30] Tao Zheng, Peilu Chen, Ting Lu, Ying Jin, and Lianguang Liu. Effects of geomagnetically induced currents on current transformer and differential protection. In *2013 IEEE Power & Energy Society General Meeting*, pages 1–5. IEEE, 2013.

[31] Emanuel E. Bernabeu. Single-phase transformer harmonics produced during geomagnetic disturbances: Theory, modeling, and monitoring. *IEEE Transactions on Power Delivery*, 30(3):1323–1330, 2015. doi: 10.1109/TPWRD.2014.2371927.

[32] Yong Liu, Yong Jia, Zhenzhi Lin, Yingchen Zhang, Lei Wang, Kevin Tomsovic, and Yilu Liu. Impact of gps signal quality on the performance of phasor measurements. In *2011 16th International Conference on Intelligent System Applications to Power Systems*, pages 1–6, 2011. doi: 10.1109/ISAP.2011.6082158.

[33] Working Group K17 K Substation Protection Subcommittee. Geomagnetic disturbances (gmd) impacts on protection systems (tr72). Technical report, IEEE Power & Energy Society, 09 2019.

[34] Qun Qiu, V Madani, Tapan Manna, T Raffield, S Klecker, Yuan Liao, S Meliopoulos, and D Fontana. Geomagnetic disturbances (gmd) impacts on protection systems. 2021.

[35] Stanley H Horowitz, Arun G Phadke, and Charles F Henville. *Power system relaying*. John Wiley & Sons, 2022.

[36] Luis Marti, Jonathan Berge, and Rajiv K. Varma. Determination of geomagnetically induced current flow in a transformer from reactive power absorption. *IEEE*

*Transactions on Power Delivery*, 28(3):1280–1288, 2013. doi: 10.1109/TPWRD.2012.2219885.

[37] R.A. Walling and A.N. Khan. Characteristics of transformer exciting-current during geomagnetic disturbances. *IEEE Transactions on Power Delivery*, 6(4):1707–1714, 1991. doi: 10.1109/61.97710.

[38] *SEL-587-0 Current Differential/Overcurrent Relay*. Schweitzer Engineering Laboratories, Pullman, WA, USA, July 2019. URL https://selinc.com/products/587/.

[39] *T60 Transformer Management Relay, UR Series Instruction Manual*. General Electrics, Markham, Ontario, Canada, 2006. URL https://www.gegridsolutions.com/products/manuals/t60/t60man-m2.pdf.

[40] Rui Fan, Yu Liu, Aniemi Umana, Zhenyu Tan, Liangyi Sun, and Yiran An. The impact of solar storms on protective relays for saturable-core transformers. In *2017 IEEE Power & Energy Society General Meeting*, pages 1–5, 2017. doi: 10.1109/PESGM.2017.8274324.

[41] Babak Ahmadzadeh-Shooshtari and Afshin Rezaei-Zare. Analysis of transformer differential protection performance under geomagnetically induced current conditions. *Electric Power Systems Research*, 194:107094, 2021.

[42] Babak Ahmadzadeh-Shooshtari and Afshin Rezaei-Zare. Advanced transformer differential protection under gic conditions. *IEEE Transactions on Power Delivery*, 37(3):1433–1444, 2022. doi: 10.1109/TPWRD.2021.3087463.

[43] Wikipedia. Solar cycle. https://en.wikipedia.org/wiki/Solar_cycle, . Accessed: 2023-03-31.

[44] A. Sicard-Piet, D. Boscher, and D. Lazaro. Is carrington event in 1859 really worse than other recent extreme events? In *2016 16th European Conference on Radiation and Its Effects on Components and Systems (RADECS)*, pages 1–6, 2016. doi: 10.1109/RADECS.2016.8093140.

[45] A. G. McNish. The magnetic storm of march 24, 1940. *Terrestrial Magnetism and Atmospheric Electricity*, 45(3):359–364, 1940. doi: https://doi.org/10.1029/TE045i003p00359.

[46] NERC NERC. Report on march 13, 1989 geomagnetic disturbance, 1990.

[47] Sebastien Guillon, Patrick Toner, Louis Gibson, and David Boteler. A colorful blackout: The havoc caused by auroral electrojet generated magnetic field variations in 1989. *IEEE Power and Energy Magazine*, 14(6):59–71, 2016. doi: 10.1109/MPE.2016.2591760.

[48] Léonard Bolduc. Gic observations and studies in the hydro-québec power system. *Journal of Atmospheric and Solar-Terrestrial Physics*, 64(16):1793–1802, 2002. ISSN 1364-6826. doi: https://doi.org/10.1016/S1364-6826(02)00128-1. Space Weather Effects on Technological Systems.

[49] Antti Pulkkinen, Sture Lindahl, Ari Viljanen, and Risto Pirjola. Geomagnetic storm of 29–31 october 2003: Geomagnetically induced currents and their relation to problems in the swedish high-voltage power transmission system. *Space Weather*, 3(8), 2005. doi: https://doi.org/10.1029/2004SW000123.

[50] Cleiton da Silva Barbosa, Gelvam André Hartmann, and Katia Jasbinschek Pinheiro. Numerical modeling of geomagnetically induced currents in a brazilian transmission line. *Advances in Space Research*, 55(4):1168–1179, 2015. doi: https://doi.org/10.1016/j.asr.2014.11.008.

[51] Bogdan Kasztenny, Normann Fischer, Douglas Taylor, Tejasvi Prakash, and Jeevan Jalli. Do cts like dc? performance of current transformers with geomagnetically induced currents. In *2016 69th Annual Conference for Protective Relay Engineers (CPRE)*, pages 1–17, 2016. doi: 10.1109/CPRE.2016.7914885.

[52] Shiyuan Wang, Payman Dehghanian, Li Li, and Bo Wang. A machine learning approach to detection of geomagnetically induced currents in power grids. *IEEE Transactions on Industry Applications*, 56(2):1098–1106, 2020. doi: 10.1109/TIA.2019.2957471.

[53] Adedasola A. Ademola, Xiawen Li, Andrea Pinceti, Micah J. Till, Kevin D. Jones, R. Matthew Gardner, and Yilu Liu. Effects-based monitoring of geomagnetically-induced current using a convolutional neural network. *IEEE Transactions on Power Delivery*, pages 1–9, 2022. doi: 10.1109/TPWRD.2022.3181250.

[54] Pavel Ripka, Karel Draxler, and Renata Styblikova. Measurement of dc currents in the power grid by current transformer. *IEEE Transactions on Magnetics*, 49(1): 73–76, 2013. doi: 10.1109/TMAG.2012.2216862.

[55] Behzad Behdani, Mohsen Tajdinian, Mehdi Allahbakhshi, Marjan Popov, Miadreza Shafie-khah, and João P. S. Catalão. Experimentally validated extended kalman filter approach for geomagnetically induced current measurement. *IEEE Transactions on Industrial Electronics*, 69(6):6316–6328, 2022. doi: 10.1109/TIE.2021.3094488.

[56] Babak Ahmadzadeh-Shooshtari and Afshin Rezaei-Zare. A waveform-based approach for transformer differential protection under gic conditions. *IEEE Transactions on Power Delivery*, 37(6):5366–5375, 2022. doi: 10.1109/TPWRD.2022.3176815.

[57] Mohamadreza Ariannik, Afshin Rezaei-Zare, and Peter Werle. Processing magnetometer signals for accurate wide-area geomagnetic disturbance monitoring and resilience analysis. *IEEE Transactions on Power Delivery*, 36(4):2550–2558, 2021. doi: 10.1109/TPWRD.2020.3024908.

[58] J.G. Kappenman, S.R. Norr, G.A. Sweezy, D.L. Carlson, V.D. Albertson, J.E. Harder, and B.L. Damsky. Gic mitigation: a neutral blocking/bypass device to prevent the flow of gic in power systems. *IEEE Transactions on Power Delivery*, 6 (3):1271–1281, 1991. doi: 10.1109/61.85876.

[59] Electrical and Computer Engineering at Washington University. 118 bus power flow test case. URL https://labs.ece.uw.edu/pstca/pf118/pg_tca118bus.htm.

[60] Aboutaleb Haddadi, Luc Gérin-Lajoie, Afshin Rezaei-Zare, Reza Hassani, and Jean Mahseredjian. A modified ieee 118-bus test case for geomagnetic disturbance studies—part ii: Simulation results. In *2020 IEEE Power & Energy Society General Meeting (PESGM)*, pages 1–1, 2020. doi: 10.1109/PESGM41954.2020.9281395.

[61] Standard Drafting Team. Benchmark geomagnetic disturbance event. 2016.

[62] Transmission system planned for geomagnetic disturbance events.

[63] Ken Behrendt, Normann Fischer, and Casper A. Labuschagne. Considerations for using harmonic blocking and harmonic restraint techniques on transformer differential relays. 2011.

[64] William L Brogan. *Modern control theory*. Pearson education india, 1991.

[65] Katsuhiko Ogata et al. *Modern control engineering*, volume 5. Prentice hall Upper Saddle River, NJ, 2010.

[66] Habib Hamdi, Mickael Rodrigues, Chokri Mechmeche, Didier Theilliol, and N Benhadj Braiek. State estimation for polytopic lpv descriptor systems: application to fault diagnosis. *IFAC Proceedings Volumes*, 42(8):438–443, 2009.

[67] Amir Ameli, Mohsen Ghafouri, Hatem H. Zeineldin, Magdy M. A. Salama, and Ehab F. El-Saadany. Accurate fault diagnosis in transformers using an auxiliary current-compensation-based framework for differential relays. 70:1–14, 2021. doi: 10.1109/TIM.2021.3097855.

[68] M Sami Fadali and Antonio Visioli. *Digital control engineering*. 2013.

[69] Gary J Balas. Linear, parameter-varying control and its application to aerospace systems. In *ICAS congress proceedings*, 2002.

[70] Hassan K Khalil. Nonlinear systems second edition. *Patience Hall*, 115, 1996.

[71] Francesco Amato and Francesco Amato. Quadratic stability. *Robust control of linear systems subject to uncertain time-varying parameters*, pages 31–92, 2006.

[72] E Martínez and R Galindo. Quadratic stability methodology by parameter dependent state feedback for lpv systems. In *2012 9th International Conference on Electrical Engineering, Computing Science and Automatic Control (CCE)*, pages 1–6. IEEE, 2012.

[73] Sana Salhi, Nedia Aouani, and Salah Salhi. Lpv polytopic modelling and stability analysis of a dfig for a wind energy conversion system based on lmi approach. In *2017 International Conference on Green Energy Conversion Systems (GECS)*, pages 1–6. IEEE, 2017.

[74] Dalil Ichalal and Saïd Mammar. On unknown input observers for lpv systems. *IEEE Transactions on Industrial Electronics*, 62(9):5870–5880, 2015. doi: 10.1109/TIE.2015.2448055.